FABRICATION AND CHARACTERIZATION OF NANOSTRUCTURED Pt AND Pt-Ag ALLOYS, AND INVESTIGATION OF THEIR HYDROGEN GAS SENSING PROPERTIES

M.Sc. THESIS

Şeyma ÜRDEM

Department	:	**NANOSCIENCE AND NANOENGINEERING**
Advisor	:	**Assoc. Prof. Dr. Mustafa ERKOVAN**
Co-Advisor	:	**Assoc. Prof. Dr. Necmettin KILINÇ**

July 2016

SAKARYA UNIVERSITY
INSTITUTE OF SCIENCE AND TECHNOLOGY

FABRICATION AND CHARACTERIZATION OF NANOSTRUCTURED Pt AND Pt-Ag ALLOYS, AND INVESTIGATION OF THEIR HYDROGEN GAS SENSING PROPERTIES

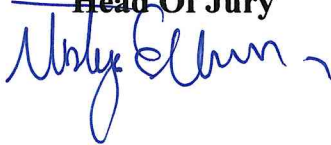## M.Sc. Thesis

Şeyma ÜRDEM

Department   :   NANOSCIENCE AND
                                       NANOENGINEERING

This thesis has been accepted unanimously by the examination committee on 13.07.2016.

Assoc. Prof. Dr.	Prof. Dr.	Prof. Dr.
Mustafa ERKOVAN	Sefer Cem OKUMUŞ	Yusuf YERLİ
Head Of Jury	JuryMember	JuryMember

DECLERATION

I declare that all the data in this thesis was obtained by myself in academic rules, all visual and written information and results were presented in accordance with academic and ethical rules, there is no distortion in the presented data, in case of utilizing other people's works they were refereed properly to scientific norms, the data presented in this thesis has not been used in any other thesis in this university or in any other university.

Şeyma ÜRDEM

13.07.2016

ACKNOWLEDGEMENTS

TABLE OF CONTENTS

LIST OF SYMBOLS AND ABBREVIATIONS

Å	:Angstrom
Ag	:Silver
Ar	:Argon
CHFCA	:Canadian Hydrogen and Fuel Cell Association
Ca	:Calcium
CO	:Carbon Monoxide
DC	:Direct Current
EDX	:Energy Dispersive X-ray Spectroscopy
FCC	:Face Centered Cubic
H_2	:Hydrogen
IDT	:Interdigitated Transducer
Mg	:Magnesium
MOS	:Metal Oxide Semiconductor
Na	:Sodium
O	:Oxygen
Pt	:Platinum
Pd	:Palladium
PVD	:Physical Vapour Deposition
QCM	:Quartz Crystal Microbalance
RF	:Radio Frequency
SAW	:Surface Acoustic Wave
SEM	:Scanning Electron Microscopy
Si	:Silicon
SiO_2	:Silicon Dioxide
SPR	:Surface Plasmon Resonance

XRD   :X-ray Diffraction

XPS   :X-ray Photoelectron Spectroscopy

LIST OF FIGURES

LIST OF TABLES

SUMMARY

Keywords: Gas Sensor, Hydrogen, Pt, PtAg Alloy

This thesis presented hydrogen (H_2) sensing properties of platinum (Pt) and platinum-silver (Pt-Ag) thin films. Pt and PtAg films were deposited on glass substrate by magnetron sputter technique. The Pt thin films with different thickness (2-50 nm) were prepared using RF sputtering method. The thicknesses of the films were controlled by a piezoelectric sensor placed in sputter system at the same time of coating process. On the other hand in this study, 3 nm Pt_xAg_{1-x} (x: 0.95, 0.90, 0.80 and 0.50) thin films were coated by co-sputtering technique. The structural properties of Pt and PtAg alloy films were characterized by X-ray diffraction (XRD), scanning electron microscopy (SEM), X-ray photoelectron spectroscopy (XPS) and energy dispersive X-ray spectroscopy (EDX) techniques. Hydrogen sensing properties of the Pt and PtAg films were investigated depending on film thickness, temperature and concentration. Temperature dependent resistances and the gas measurements of the Pt and PtAg thin films were studied under a dry air flow and hydrogen ambient at a temperature range from 30 °C to 200 °C. Thus the best working performances of Pt and PtAg sensors were detected.

The results showed that the resistance is directly proportional with temperature, and inversely proportional with the thickness of Pt thin film sensors. The H_2 sensing properties of Pt thin film sensors were examined in the concentration range of 0.1 % - 1 % H_2. Among the results for Pt thin films, it was revealed that the Pt thin film with 2 nm thickness exhibited the best sensing performance to H_2 at 30 °C under dry air flow. The best response time was obtained at high temperatures for Pt thin film sensors. H_2 sensitivity of PtAg sensors were also investigated in the concentration of 25 ppm - 1000 ppm H_2. The resistances and the sensitivities of PtAg thin film sensors were increased with enhancing the temperature. Among the results for PtAg sensors, 3 nm $Pt_{0.80}Ag_{0.20}$ sensor showed the best sensitivity properties at 150 ºC.

NANOYAPILI Pt VE Pt-Ag ALAŞIMLARININ ÜRETİMİ, KARAKTERİZASYONU VE HİDROJEN GAZ ALGILAMA ÖZELLİKLERİNİN İNCELENMESİ

ÖZET

Anahtar kelimeler: Gaz Sensör, Hidrojen, Pt, PtAg Alloy

Mevcut tez çalışması, platin (Pt) ve platin-gümüş (Pt-Ag) alaşım ince filmlerin hidrojen gaz algılama özelliklerini incelemiştir. Pt ve PtAg filmler cam alttaş üzerine magnetron sputter tekniği ile kaplanmıştır. Her biri farklı kalınlığa sahip Pt filmler (2-50 nm) RF sputtering yöntemi kullanılarak hazırlanmıştır. Kaplama sırasında filmlerin kalınlık kontrolü sputter sistemi içerisinde bulunan piezoelektrik sensörle yapılmıştır. Çalışmada ayrıca, 3 nm Pt_xAg_{1-x} (x: 0.95, 0.90, 0.80 ve 0.50) ince filmler co-sputtering yöntemi kullanılarak kaplanmıştır. Pt ve PtAg alaşım filmlerin yapısal karakterizasyonları X-ışını kırınımı (XRD), taramalı elektron mikroskobu (SEM), X-ışını fotoelektron spektroskopisi (XPS) ve enerji dağılımlı X-ışını spektroskopisi (EDX) teknikleri ile yapılmıştır. Pt ve PtAg filmlerin kaplama kalınlığına, sıcaklığa ve konsantrasyona bağlı hidrojen duyarlılıkları incelenmiştir. Pt ve PtAg ince filmlerin sıcaklığa bağlı direnç değişimleri ve gaz ölçümleri ise kuru hava ve hidrojen ortamında 30 °C ile 200 °C arasında değişen sıcaklıklarda test edilmiştir. Böylece Pt ve PtAg sensörler için en iyi çalışma performansları belirlenmiştir.

Elde edilen sonuçlar, üretilen Pt ince film sensörlerde direncin sıcaklıkla doğru orantılı, kaplama kalınlığı ile ters orantılı olacak biçimde değişiklik gösterdiğini ortaya koymaktadır. Pt ince film sensörlerin % 0.1 - % 1 konsantrasyon aralığında hidrojen gazına duyarlılıkları incelenmiştir. Pt ince filmler arasında, 2 nm Pt filmin 30 °C' de ve kuru hava ortamında en iyi duyarlılık performansı gösterdiği görülmüştür. Pt ince film sensörlerin en iyi cevap süresine ise oldukça yüksek sıcaklıklarda ulaştığı saptanmıştır. PtAg sensörlerin H_2 duyarlılıkları 25 ppm – 1000 ppm hidrojen konsantrasyon aralığında incelenmiştir. PtAg ince film sensörlerin direnç ve duyarlılığı sıcaklığın artması ile birlikte artmıştır. PtAg sensörleri arasında en iyi çalışma performansı ise 3 nm $Pt_{0.80}Ag_{0.20}$ sensör için 150 °C'de görülmüştür.

CHAPTER 1. INTRODUCTION

In recent years, the industrialization of world has caused series of problems which are related with the technological developments. The industrial processes have involved increasingly the use of highly dangerous, toxic and combustible gases. In some cases, gas escapes may occur in the places gases were used. The gas escapes cause a potential hazard for the industrial factories, workers of the plants, and also people living nearby. Gas leakage causes some disastrous incidents and consequences for people such as asphyxiation, explosions and even loss of life. The increasing usage of gases in industrial processes makes it absolutely necessary to control air pollution in several areas such as environment, factories, hospitals, laboratories and many more. All these problems mentioned above have led to produce gas sensor devices. Gas sensors help to prevent caused from gas escapes and thus it plays a key role in various technological processes [1, 2].

1.1. The Role Of Gas Sensors In Industry

Gas sensors are smart devices which help to prevent the problems caused from escape of gas. Sensor technology has evolved inevitably over the recent years and thus it is becoming an indispensable technology. Sensors play an important role in various modern technological processes, where control of gases are necessary. Gas sensors have become more significant because of its common applications in various areas such as the chemical and petrochemical industries, food quality control, semiconductor manufacturing, agriculture, power generation, fabrication industries including the motor, ship, and aircraft industries [2].

The atmospheric air includes several kinds of natural and synthetic chemical species. Some of the species are vital but many others are harmful to human life [3]. Therefore, the monitor of toxic and harmful gases has become a critical issue. Gas sensors control the contents of the dangerous gases in atmosphere. Therefore this smart artifacts improve our quality of life with their wide applications.

1.1. Requirements For An Ideal Gas Sensor

An ideal gas sensor could be thought to have the following characteristics [4]:

- Rapid response time and reversibility
- High sensitivity
- Compact size
- Chemical selectivity
- Wide operation temperature

CHAPTER 2. HYDROGEN GAS SENSORS

One of the widely used application areas of the gas sensor is hydrogen technology. Today several researchers have focused on novel methods to develop next generation hydrogen gas sensor having the necessary requirements such as reliable, low cost, compact size and low power consumption.

2.1. Approaches Of Nanoscience And Nanotechnology For Hydrogen Detection

Nanoscience and nanotechnology include the manipulation of materials in the atomic level to enhance material properties. This leads several innovations in processing of materials. One of the main applications of nanotechnology is sensor technologies. In this respect, nanoscience has a profound effect on every field of study that will conspicuously change and revolutionize hydrogen gas sensors [5]. Usage of nanostructured materials assure the dramatic changes in sensor capabilities and their designs. Low weight, smaller size, higher sensitivity, low power consumption and better selectivity are some of improvements of nanosized materials in sensor design [6].

There are several kind nanomaterials used for hydrogen sensors. Carbon nanotubes, nanoparticles, nanowires, nanowhiskers, metallic nanotubes, metal oxide nanostructures, and nanoclusters are some of the nanomaterials investigated for hydrogen sensing. Most of these materials are nanoscale components of bulk materials, which have been investigated for hydrogen sensing for several years. Nanomaterials have high surface to bulk ratio resulting in higher sensitivity, faster response time, and high selectivity in comparison with their bulk counterparts [7].

2.2. As An Alternative Energy Source: Hydrogen

After the present of Industrial Revolution, inexpensive and abundant resources have fueled technological advances. Growing of technology will require a supply of inexpensive energy which is not sustainable with current resources. In addition, concerns about greenhouse gas emissions from fossil fuel sources are generating a new set of technological requirements [8]. Thus in recent years, several studies have focused on searching for the new fuel source having zero emission and also being abundant in nature. Hydrogen, which is the third most abundant element on the earth's atmosphere, meets all these fuel requirements perfectly. Hydrogen generation has the potential of being inexpensive, effective and coupled with the fact that it is renewable makes it an attractive choice as fuel in various applications [9, 10].

Recently, hydrogen has received much attention because of its use as a clean energy source and therefore it has viewed as the fuel of the near future. The energy supplied by hydrogen is high. The energy amount produced by hydrogen per unit weight of fuel is about three times the energy contained nearly seven times that of coal and in an equal weight of gasoline [9].

Hydrogen has a great potential as a process gas in many industrial and technological applications such as chemical, food, metallurgy, electronics, medical and petroleum etc.[1]. Today there has been a wide market share of hydrogen consumption. According to the report of the Canadian Hydrogen and Fuel Cell Association (CHFCA), the global hydrogen and fuel cell market is poised to be worth $8.5 billion by 2016 [11]. Market share of hydrogen consumption in terms of application details are shown by Figure 2.1.
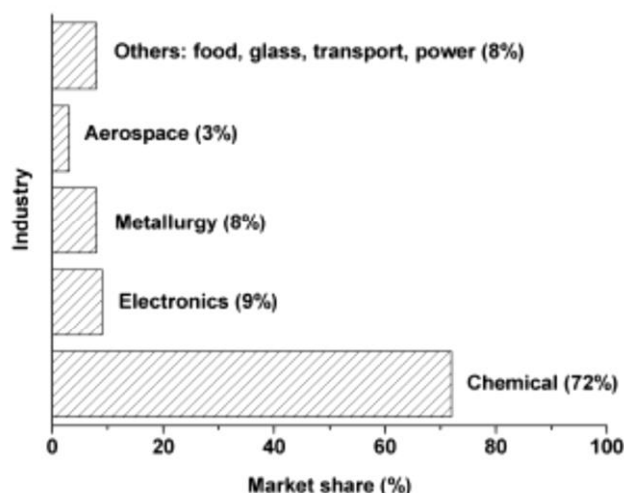
Figure 2.1. Market share of hydrogen consumption in terms of application areas [12]

2.3. Hydrogen

The promising use of hydrogen help to meet the growing energy demand. However in order to implement this, hydrogen monitoring and leak detection systems are needed. Because hydrogen has many different properties compared with other flammable gases. Hydrogen is colorless, odorless and tasteless gas. It cannot be detected by human senses. Hydrogen is explosive in a wide range of concentrations, from 15 % to 59 %, at normal atmospheric pressure. It is flammable at the concentrations between 4 % and 75 % in air [13].

In comparison with other fuels, hydrogen is actually far less dangerous than the gasoline and methane, as summarized in the Table 2.1. However, small size of the hydrogen molecule causes the gas to diffuse rapidly and permeate easily through various materials. Low mass and high diffusivity features of hydrogen make it difficult to store and use safely. A sensitive leak detection system is therefore crucial for the hydrogen safety [14].

Table 2.1. Basic safety relevant properties of combustibles [15, 16]

Properties	Hydrogen	Methane	Gasoline
Limits of flammability in air (vol %)	4-75	5-15	1.0-7.6
Auto-ignition temperature (°C)	585	540	228-471
Minimum energy for ignition in air (μJ)	20	290	240
Flame propagation velocity (ms^{-1})	3.46	0.43	--
Diffusion coefficient in air(cm^{2}s^{-1})	0.61	0.16	0.05

Regarding all these cases about the hydrogen, it is clear why it is require to create a new hydrogen monitoring system. The need for robust, affordable and compact hydrogen sensor is driving the development of new sensor technology [17]. There is a need for reliable, low cost, portable, highly specific hydrogen gas sensors which are capable of detecting the presence of dangerous levels of hydrogen [18].

2.4. Hydrogen Gas Sensors

The main object of hydrogen gas sensor is to provide reliable informations about the chemical composition of the surrounding environment. Therefore, a sensor designed for gas sensing should operate continuously and reversibly. Hydrogen sensor should produce a measurable signal output at wide range of gas concentration. It should be instantaneously selective to the hydrogen gas. Simple fabrication, fast response, relative temperature and humidity insensitivity are also useful requirements of the designed hydrogen sensor. For portable applications, an ideal H_2 sensor should be small size, has low energy consumption and it should provide repetitive measurements of target hydrogen gas for a long time [2].

2.5. Types of Hydrogen Sensor

Mass spectrometers, gas chromatographs and specific ionization gas pressure sensors are some of the examples of traditional hydrogen gas detectors. However these sensors have some shortcomings such as high cost, large size, slow response time, sometimes working at elevated temperatures. A good hydrogen sensor is required smaller size, low cost, low power consumption, fast response time and work even at room temperaure for widely use as portable and in-situ monitoring. Hydrogen economy has developed rapidly and the number of researches on promoting new types of hydrogen gas detector have increased [19].

Currently, several types of hydrogen sensor have been commercialised to find the best working sensor perfomance. Hydrogen sensors can be classified into six main types according to the gas sensing mechanism of the sensor such as electrochemical,

catalytic, thermal conductivity, surface acoustic wave, metal oxide and resistive metal based hydrogen sensors.

2.5.1. Electrochemical hydrogen sensors

Electrochemical hydrogen sensors consist of three-electrode system, an electrolyte solution and a selective membran. The potential difference occurs between the electrodes and hydrogen concentration because of the chemical reactions on the gas sensor surface. The basic representation of electrochemical sensor is given by Figure 2.2.

Electrometer
Electrical leads

Glass seal
Inert packing material

Ti/H or Zr/H reference electrode
Pt coating at reference electrode
$CaZr_{0.9}In_{0.1}O_{3-\delta}$ solid electrolyte
Pt coating at measuring electrode
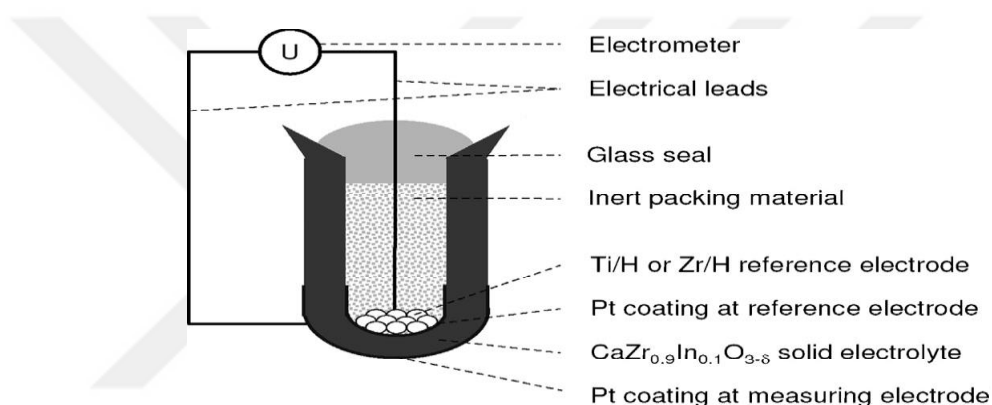
Figure 2.2. Electrochemical hydrogen sensor [20]

Electrochemical hydrogen sensors are widely used as a commercially in industry. Electrochemical sensors require very little power to operate and they are have fast response time. The life expectancy of the sensor is highly dependent on the environmental contaminants, temperature, and humidity [21]. These sensors cannot be operated at low pressures or at sub-zero temperatures [14]. Moreover electrochemical hydrogen sensors have high cost, limited lifetime and also cross sensitive to CO.

2.5.2. Catalytic hydrogen sensors

Catalytic hydrogen sensors are based on the temperature change occuring because of exothermic oxidation on heated surface of the sensor film. The principle of catalytic

sensor is based on heating up a catalytic surface to its working temperature as shown in Figure 2.3. If a combustible hydrogen gas is provided in the environment, it will react with oxygen to water. This exothermic reaction leads to a higher temperature [22]. There are two pellistors of the sensor surface which are connected by a Wheatstone bridge.
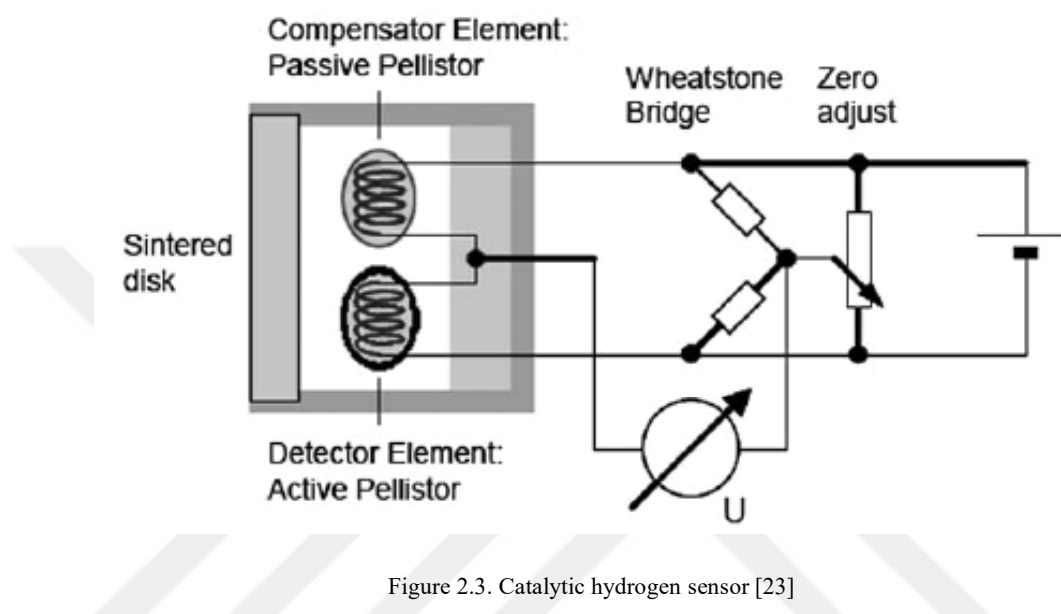
Figure 2.3. Catalytic hydrogen sensor [23]

Catalytic sensors work at a wide operating temperature. However these sensors are not selective completely to hydrogen gas. Also the sensor needs oxygen between 5 % and 10 % in the atmosphere to work exactly.

2.5.3. Thermal conductivity sensors

Thermal conductivity hydrogen sensors are based on measuring the heat lost from a resistive element to the walls of the sensor. The sensor is thermostatically maintained at a certain temperature, while the resistive element is maintained at a higher temperature. The temperature of the sensor depends on heating lost to the lower temperature. The electrical resistance of the heated sensor is measured by using Wheatstone bridge [24]. The schematic representation of thermal conductivity sensors is given by Figure 2.4.
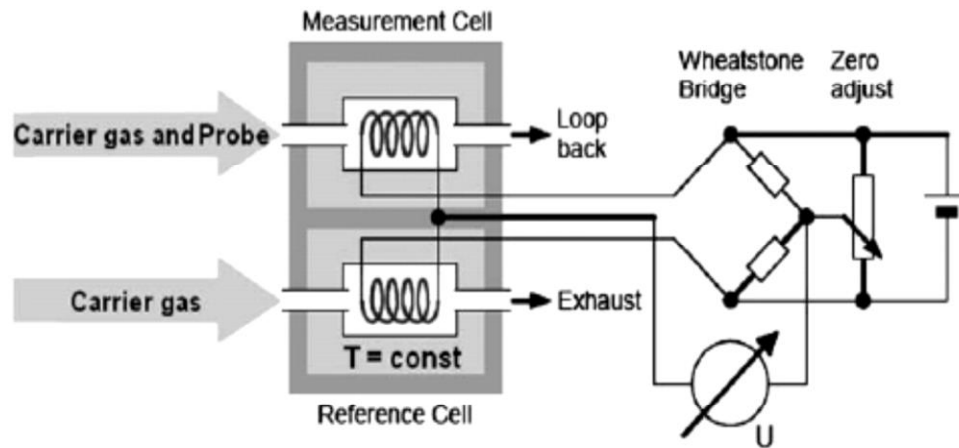
Figure 2.4. Thermal conductivity hydrogen sensor [4]

Thermal conductivity sensors are inexpensive and have resistivity to poisoning. Also the configuration of the conductivity sensors are simple. However the detection limits of the thermal conductivity hydrogen sensors are very low. They are not able to measure low concentrations and also they have cross sensitivity to helium gas.

2.5.4. Surface acoustic wave hydrogen sensors

Surface acoustic wave (SAW) hydrogen sensors operate by using interdigitated transducer (IDT). The IDT transducer is used to transform radio frequency (RF) signals into an ultrasonic electrochemical wave and vice versa a piezoelectric transduction process in a piezoelectric crystal [25]. SAW sensors are sensitive to the changes of the boundary conditions of the propagating wave. These waves are introduced by the interaction of an active thin film with hydrogen molecules. Figure 2.5 demonstrates the working principle of the surface acoustic wave sensor.
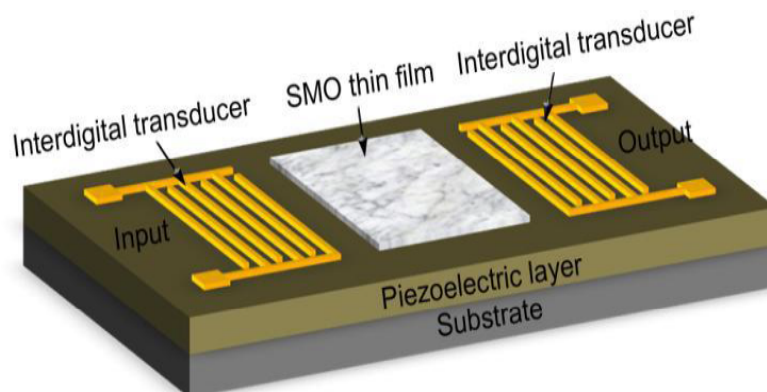
Figure 2.5. Surface acoustic wave hydrogen sensor [19]

Surface acoustic wave sensors provide desirable characteristics for hydrogen detection due to their small size, low cost, ease of integration and high sensitivity. On the other hand, SAW sensors are highly dependent to temperature and humidity [26].

2.5.5. Metal oxide hydrogen sensors

Hydrogen detection mechanism of metal oxide sensors includes a two-step process. In the first step, ambient oxygen gas is adsorbed on the defect surfaces of the metal oxide layer. In the second step, hydrogen gas diffuses to the metal oxide surface to react with the adsorbed oxygen. An electron transfer is occured into the metal oxide due to the this oxidation reaction. This electron transfer process is detected as a change in conductivity. Besides conductivity change is caused from the decrease in energy barrier of the metal oxide. Metal oxide semiconductors (MOS) have a capability of broad hydrogen gas detection. However they are not selective to hydrogen exactly and they have high power consumption. In addition the surrounding gas environment has an effect on the concentration of hydrogen recorded by the detector [27]. The basic principle of metal oxide sensor is shown in Figure 2.6.
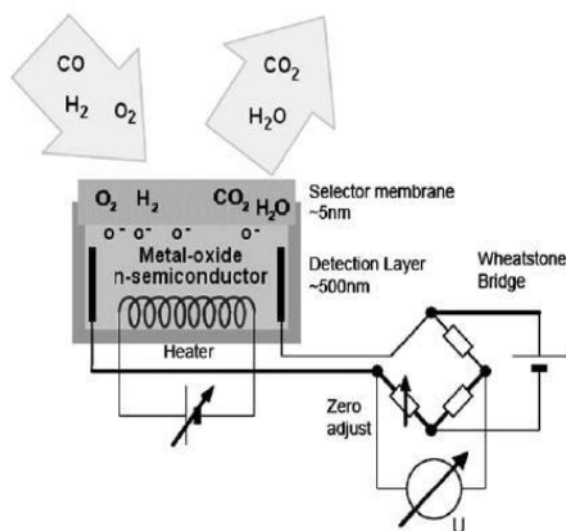
Figure 2.6. Metal oxide hydrogen sensor [23]

2.5.6. Metallic resistive hydrogen sensors

Detecting the best sensitive hydrogen gas sensor is one of the most frequently discussed topics regarding of all types of H_2 gas sensors. In this respect, advantages or disadvantages of hydrogen sensors should be evaluated. In terms of the working characteristics of gas sensors, every type of sensor has some specific disadvantages. For instance, metal oxide-based hydrogen sensors are high sensitive to air humidity and have low selectivity. Because of the surface effects of metal oxides, these sensors can transform a dormant form after several days of inactivity. Thermal conductivity sensors are not able to measure low concentrations of hydrogen. Electrochemical hydrogen sensors have a short lifetime and high cost, so they are becoming unpopular. However, there is an another type of hydrogen sensor: metallic resistive sensors. In comparison with other sensors, resistive hydrogen sensors are small size, have excellent sensitivity, low cost, short response time, low power consumption for adequate battery life and very good suitability for portable usage [2]. Because of these advantages of metallic resistive hydrogen sensors, our study was devoted to investigate metallic resistive sensor properties of Pt and PtAg thin films.

CHAPTER 3. METALLIC RESISTIVE HYDROGEN SENSORS

Metallic resistive sensors appear to have a promising future due to their unique properties in the detection of hydrogen gas quickly and accurately. Resistive hydrogen sensors have a simple structure in terms of compact size and operating mechanism. The working principle of resistive sensors is simply based on the change of electrical conductivity of the device in hydrogen ambient and absence of H_2 [2]. The change is transformed into an electrical signal by using a proper transducer. The conductivity is measured as a current change and it is related with the concentration of hydrogen gas [2, 6].

3.1. Sensing Materials For Resistive Sensors

A sensing material is a substance that changes its physical or chemical properties according to the variation of hydrogen concentration in the ambient. Sensing materials always have a significant effect on the sensing characteristics and it plays a key role in the successful implementation of resistive hydrogen sensors. In order to support an effective resistive gas sensors, some parameters are needed such as sensitivity, accuracy, fast response time, low power consumption etc. Almost all these parameters are connected with the exact sensing material used in resistive sensor. Therefore the selection of optimal sensing material is one of the most important criteria for hydrogen detection for resistive sensors.

3.2. Literature Review

Most of the studies covering the resistive hydrogen sensors are generally devoted to analysis of one spesific sensing material, Palladium (Pd). Palladium and its alloys have been extensively used as a sensitive material for the resistive hydrogen sensor. There have been lots of studies try to explain the mechanism of hydrogen gas

response based on Palladium metal [28 - 32]. However these studies have shown that there are some disadvantages of Pd when it is used as a sensing material. Palladium has been shown that high concentrations of hydrogen destruct it by blistering and big efforts have been made to stabilize it by modification [33]. Although Pd is a stable metal in air, it is oxidized at high temperatures. Therefore there are few Pd-based resistive sensors which operate at above room temperature because of the oxidation of Pd.

Figure 3.1. Elements arranged closely to palladium in the periodic table [34]

Regarding all the shortcomings of Pd metal as a sensing material, the efforts to improve the selectivity of resistive hydrogen sensors have been focused on searching for new sensing materials. In the periodic table, among the candidate metals as shown in Figure 3.1, platinum has higher catalytic activity than palladium. Pt is thought to be stable because of its low hydrogen diffusion as compared to palladium [36]. Platinum provides stable and fully reversible signals even at room temperature. Also, a wide detection range is available and very fast response times are observed at the room temperature by using Pt [33].

Despite all these promising features of platinum, there has been quite limited studies about the Pt based hydrogen sensors [35-39]. The study of Yang et al. [37] is a good example in that the comparison Pd and Pt as a sensing material for hydrogen gas

sensor. They synthesized Platinum (Pt) and Palladium (Pd) nanowires by electrodeposition method. They compared the Pt and Pd nanowires based on the sensing mechanism of hydrogen. The experiments showed that single Pt nanowire was more sensitive than Pd nanowire. A Pt nanowire was able to detect H_2 at much lower concentrations (down to 10 ppm) than a Pd nanowire of the same size. However the problem of the study is that the response and recovery time of Pt was lower than Pd at all H_2 concentrations. Patel et al. [39] worked on the structure and hydrogen-induced conductometric response of thin particulate Pt films. They deposited 35 Å Pt films on SiO_2 surface by electron-beam evaporation. They investigated H_2 sensitivity depend of the temperature and concentration. 5 % oxygen was used with nitrogen as a carrier gas. The results indicated that the electrical resistance of Pt film decreased in the presence of hydrogen. However, the H_2 sensitivity of Pt increased with increasing the temperature. Abburi et al. [38] studied on the fabrication of nanoporous Pt films and its application as hydrogen sensors. They demonstrated that the resistivity of nanoporous Pt film increased when the film surface exposed to hydrogen gas. The increase in resistivity has explained with the forming of PtHx hydride phase. Also, they indicated that there is no need any oxygen to detect H_2 gas via nanoporous Pt films. Among these studies, the sensing mechanism of Pt resistive hydrogen sensor is not fully understood. The working the principles of the sensors have been explained differently and controversially. One of the study [39] has supported an idea that the resistivity of Pt decreases with the increasing of hydrogen. On the contrary, the other work [38] has proposed that the resistivity of Pt increases in the presence of hydrogen.

Moreover, in the most of the researches about Pt-based hydrogen sensors, it is observed that sensors have two main shortcomings such as low sensitivity and operation at high temperature. While some of the studies have focused on sensitivity, the others have studied about the operating temperature. High sensitive sensors generally work at high temperatures. This situation causes the increasing of the power consumption [40]. On the other hand, the sensors which operate at the low temperatures are not sensitive enough to the detection of hydrogen.

The aim of the thesis is to overcome these shortcomings in this regard and to reveal the sensing mechanism of hydrogen gas detection by utilization of Pt and Pt-Ag alloy. The thesis has demonstrated that the low concentration detection of hydrogen even at room temperature is fabricated by using Pt as a sensing material having high sensitivity. Fast, economic and easy preparation techniques have been used to obtain Pt nanosized thin film as a sensing material. It has been examined the role of the noble metal platinum as a catalyst to reveal that the Pt based hydrogen sensors is the best sensitivity in a wide range of temperature. Also one of the main object of this thesis is to explain the sensing mechanism of hydrogen detection and, thus to create low cost and low power hydrogen gas sensor working at room temperature.

Until now there has been no study about PtAg alloys in the application of hydrogen sensor to our knowledge. So the thesis will be the first study about PtAg alloy thin films used in hydrogen sensors. It is expected that the dissertation will provide useful guideliness on H_2 gas sensor. The succesful utilization of Pt and Ag nanoparticles for hydrogen detection makes several contributions in hydrogen gas sensor technology.

CHAPTER 4. EXPERIMENTAL TECHNIQUES

4.1. Deposition Techniques

Thin film technology is one of the main application area of the solid-state electronics. Especially the usefulness of metal films in a wide range of the scientific and technological applications has promoted interest in studying of thin films [41].

As a general term, thin film is a layer which is condensed the species on the surface. The range of thin film thickness is between the nanometer and micrometer. The growth process of the thin films has great importance due to the fact that thin film processing influences the film thickness, physical structure of the substrate. According to the properties of bulk material, some deviations can occur due to physical structure, large surface to volume ratio and also small thickness of the films. All these criterias about the thin film growing may effect gas adsorption-desorption process and catalytic activities of the films [42].

There are several thin film coating techniques such as pulsed laser deposition [43], chemical vapor deposition [44], dip-coating technique [45] and magnetron sputtering deposition [46]. Among these techniques, magnetron sputtering deposition has become one of the most common methods to fabricate thin film due to its advantages of coating uniformly and higher sputter rate and continuity of the films.

4.1.1. Sputtering technique

Sputtering is a term used to describe the process of ejection of atoms from a solid target material by making bombardment of the target using particles having high energy [47].

Sputtering deposition is a physical vapor deposition technique (PVD) and it has widely usage area for scientific and industrial areas. Sputtering is generally used in coating applications such as optical, biomedical or electronic device industry. Metals, alloys, ceramics or multilayer materials can be deposited successfully by the sputtering. The technique provides high quality functional film coating and it has several advantages. Materials having very high melting points are sputtered easily. Sputtered films have good adhesion and low roughness layer on the substrate. Low friction, corrosion resistant and wear resistant coatings are produced by the sputtering technique [48].

4.1.1.1. Mechanism of sputtering

Sputtering system consists of a power supply, a substrate (anode compartment) material to be coated and a target material (cathode compartment) applied negative potential. Sputtering process needs vacuum conditions to fabricate higher quality films. In sputtering process, a substrate material and target material are placed in a vacuum chamber including an inert gas. Plasma medium is created by ionizing inert gases, generally Argon gas is used. The coating process begins when the target material is bombarded by the ions of Argon gas. Firstly, neutral Argon atoms impact with free electrons released from the target in the plasma. Thus, inert gas atoms become positively charged ions and formed Ar^+ ions. Argon ions dislodge the atoms of the target material on the surface. The surface of coating material is vaporized by the ion bombardment and atoms are sputtered from the target. The repelled atoms start to move from the target to the substrate in plasma medium. The ejected atoms are deposited and formed a film label on the substrate surface. The process continues until the surface of substrate material is completely coated [49, 50]. The principle of the sputtering process is shown in Figure 4.1.
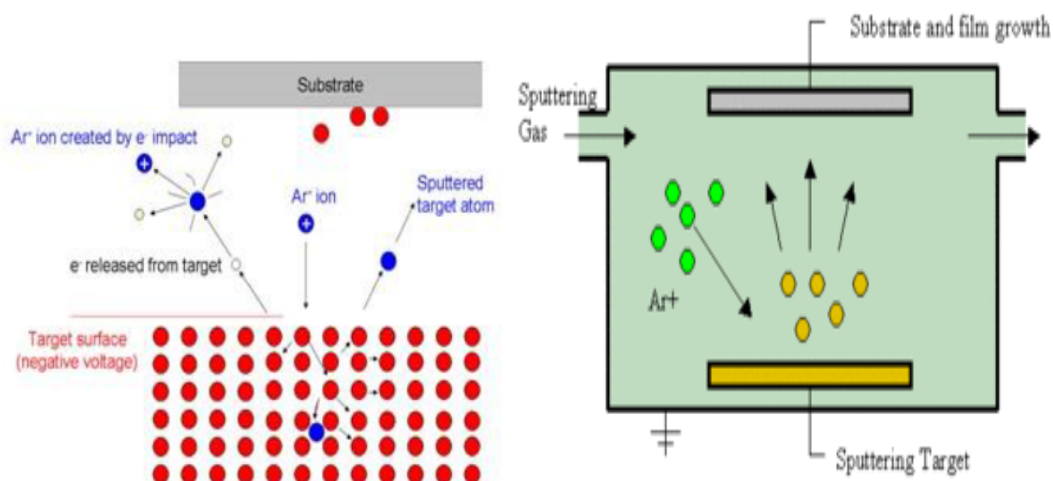
Figure 4.1. The principle of sputtering technique [51, 52]

4.1.2. Magnetron sputtering deposition

Despite the sputtering process is a widely used technique in material deposition, it has some dificulties in practice such as low ionisation effect in the plasma medium, low rate of deposition, and increasing of substrate temperature because of the plasma. Moreover the ion bombartment can cause overheating and the structural damages in the substrate to be coated can be observed. Therefore a magnetic field was placed in a vacuum system to overcome all the problems of sputtering. Magnetic field is used to control ion velocity and behavior by using the property of ions that are charged particles in magnetron deposition. In the magnetron sputtering process, free electrons are trapped above the target surface aided by the magnets and confined above the target. Hence it is prevented to escape the free electrons from out of the magnetic field and to attact these electrons toward the substrate to be coated. Via the magnetic field it is produced to confine and to keep the plasma going near the target. In this way the damages are induced in thin film formation on the substrate surface [49, 50].

In magnetron deposition, a voltage source (DC, RF) is placed behind the target material and a negative electrical potential is applied to the target. The electrical potential cause free electrons to accelerate away from the magnetron. When Argon atom collides with these free electrons, positively charged Argon ions (Ar$^+$ ions) and

secondary electrons are created caused from a strong potential difference. The secondary electrons are confined near to the target compartment. Argon ions are accelerated toward the magnetron and the atoms of the target surface are sputtered. Target atoms move to the substrate forming a thin film or coating. The sputtered atoms are neutrally charged. They are not affected by the magnetic trap. The sputtering process continues until the thin film formation occurs onto the substrate surface. Figure 4.2 shows the schematic illustration of the magnetron sputtering system.
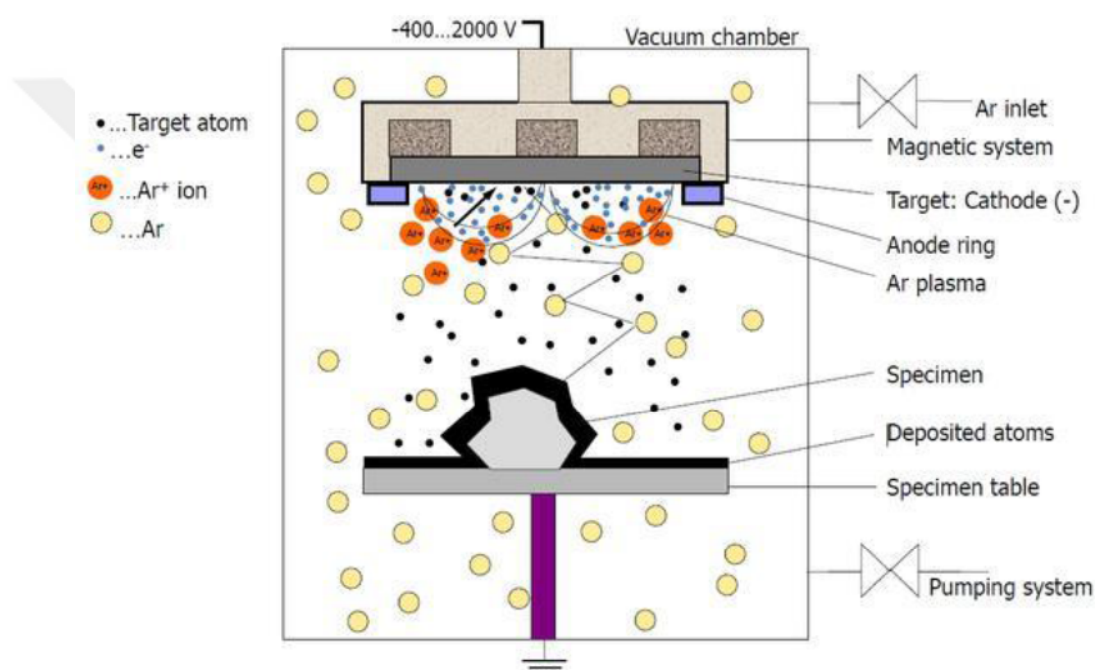
Figure 4.2. Schematic representation of magnetron sputtering system [53]

4.1.2.1. Co-sputtering deposition

Co-sputtering is a type of magnetron sputtering. In co-sputtering system, two different target material are used and sputtered simultaneously in the reactive gas ambient. Target materials are controlled independently by using two different supplies. Co sputtering process is generally accomplished with the use of DC or RF power supplies, as shown in Figure 4.3. The chemical composition ratios of target metals are controlled with the power of each the magnetrons in the sputtering system [54].
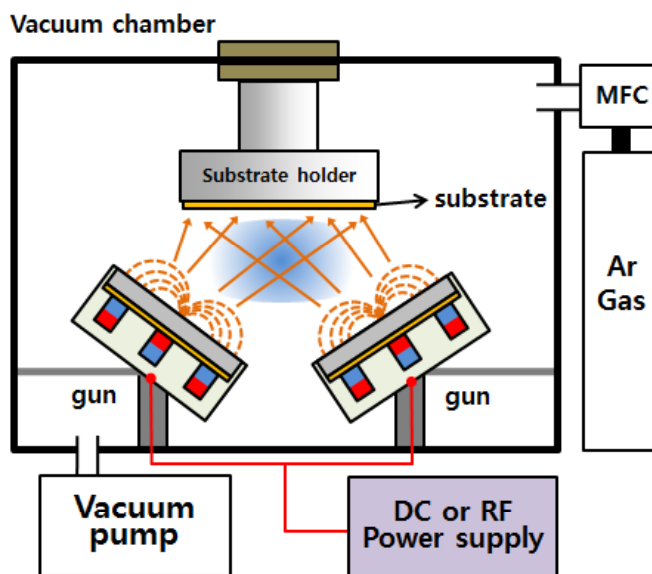
Figure 4.3. Figure of co-sputtering deposition system [55]

4.2. Characterization Techniques

Structural and electrical characterization measurements are carried out for examining the characteristic behaviour of the nanostructured films and the sensor responses such as sensitivity and selectivity. The structural characterization of the films were investigated by scanning electron spectroscopy (SEM), X-ray photoelectron spectroscopy (XPS), X-ray diffraction (XRD) methods. The electrical characterizations of the device was indicated via four point method. The sensor measurement system was adjust to detect the gas sensing principle of the device.

4.2.1. X-ray photoelectron spectroscopy (XPS)

X-ray Photoelectron Spectroscopy (XPS) is also called the name of Electron Spectroscopy for Chemical Analysis (ESCA). However, today it has generally been used by the more spectroscopically term of X-ray photoelectron spectroscopy [56].

XPS is one of the most widely used surface analysis technique in order to obtain a complete decription of surface. XPS gives informations about qualitative elemental

analysis and quantitative composition of material from the surface to a few nanometers. X-ray photoelectron spectroscopy irradiates the sample surface with a soft or hard X-ray source. The technique is non-destructive for the surface [57].

The technique requires ultrahigh vacuum conditions ($P < 10^{-9}$ mbar) to protect the surface of sample without any contamination during the experimental process. The chemical compounds on a sample surface are investigated using monochromatic X-ray incident beams. Thus it is aimed to be prevented any stray X-rays other than applied eV. Al Ka (1486.6 eV) or Mg Ka (1253.6 eV) are often used the photon energies in XPS. X-ray radiation is applied to induce electrons from their core levels. XPS gives the depth information near the sample surface. The analysis is circa sensitive in the first 10 nm [58].

XPS is based on photoelectric effect and the interactions between X-ray and electrons. As incident X-ray collides with a core electron, if X-ray energy is high enough, electrons can be emitted from the sample. X-ray photon with a sufficient energy excites the electron of the atom and causes emission of electon from its electronic shell. The electron is emitted as a photoelectron if the binding energy is lower than X-ray energy. Then it is created a core-hole through the absorption of incoming light with energy matched to the binding energy of a core electron. The core electron excites to a bound state or to a state where it becomes free. The electron is released with a certain kinetic energy that is directly related to the binding energy of the electron to the atom when it exposed to X-ray photon (Figure 4.4.) [59].
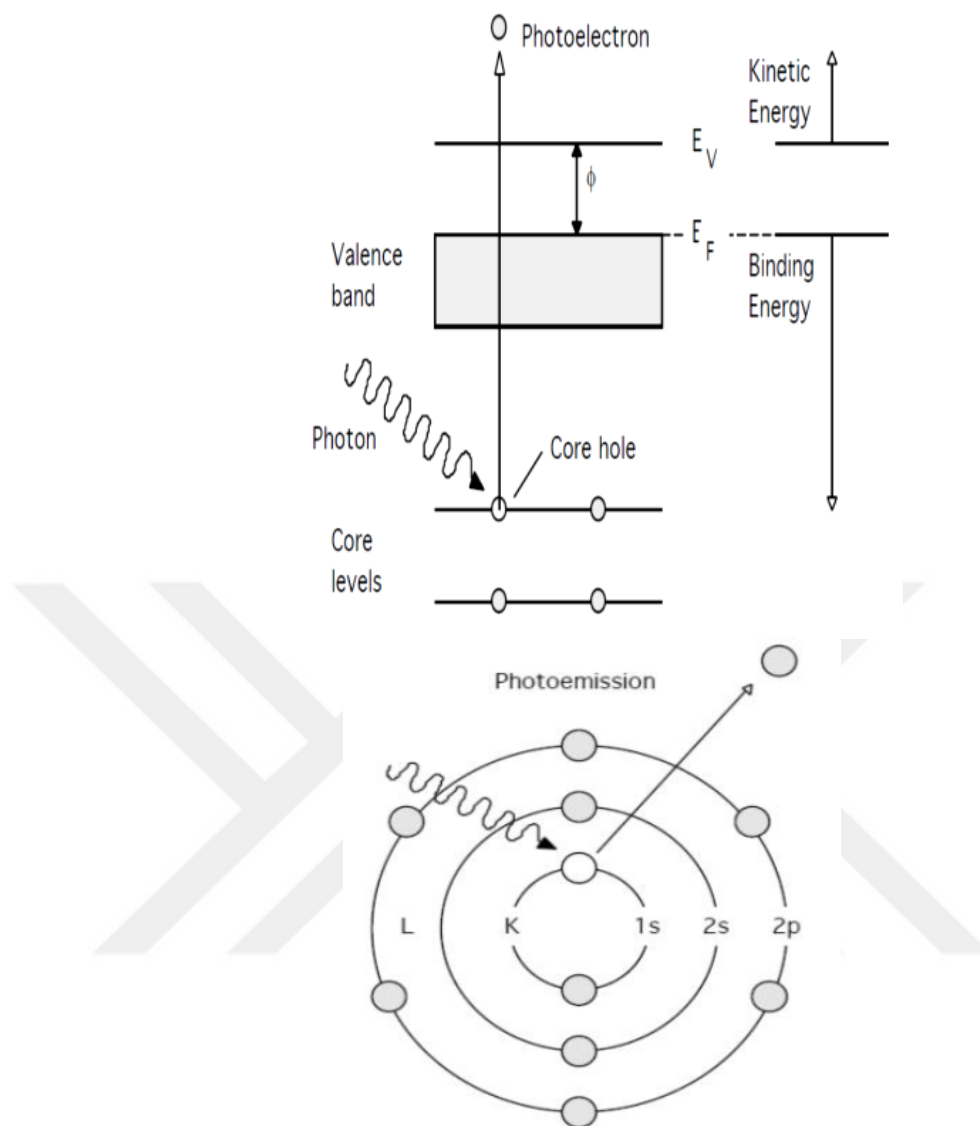
Figure 4.4. Photoemission process of an electron [60]

The energy balance of the photoemission process is formulized as in the Equation 4.1.

$$h\nu = KE + BE + \phi \tag{4.1}$$

The equation shows: $h\nu$ is the energy of the X-ray photons being used, KE is the kinetic energy of the emitted electron, BE is the binding energy of the electron and ϕ is the work function of the spectrometer.

If the binding energy of the electron is smaller than photon energy, the excess energy is converted to the kinetic energy of the emitted photoelectron [59].

The ejection of the core electron creates a highly energetic unstable hole in the electronic shell. This inner-shell vacancy is filled by a second electron from an outer shell. During this relaxation process an energy is released and the gained energy is transmitted to another outer shell electron, Auger electron, which lead to Auger emission. This released energy is used to emit the third electron with a lower binding energy compared to the second electron (Figure 4.5).
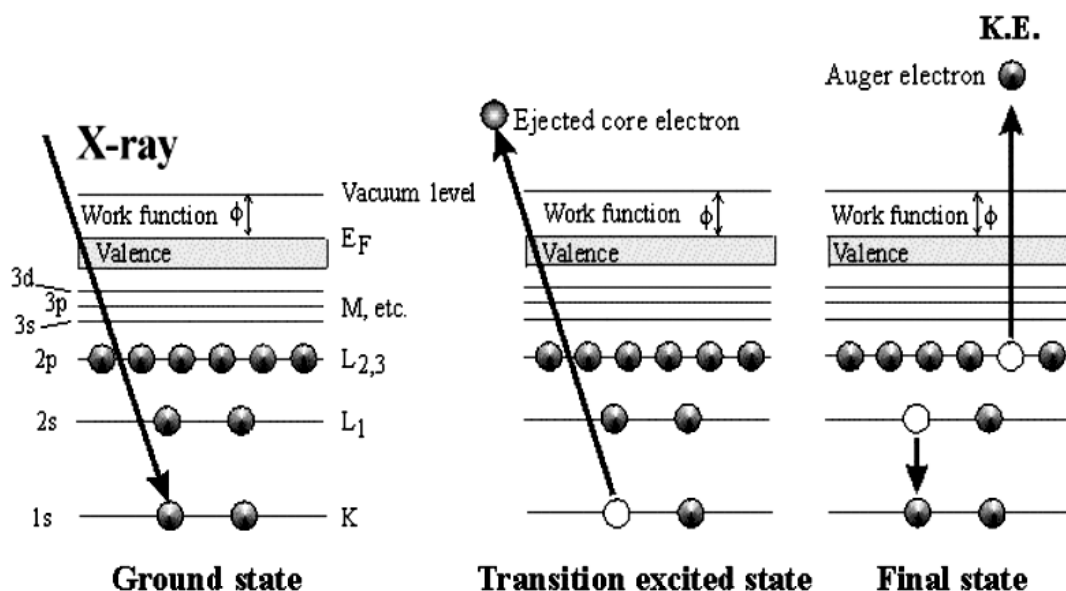
Figure 4.5. The process of Auger emission [61]

The kinetic energy of Auger electron is independent from X-ray photon energy which spent for the creation of the core hole [62]. The kinetic energy depends only on the energy separations of the levels involved. Therefore the kinetic energy of Auger electrons is much lower than the one of photoelectron energy. Auger peaks accompany to XPS peaks and they are recorded during XPS experiment. X-ray excited electron peaks and Auger electron peaks contain important informations about the chemical state of the atoms involved.

The electron orbitals of an atom have different binding energies. XPS is used to identify the element composition of the sample. Because the binding energies of the electrons are characteristic for every element as their fingerprint. The binding energy of the electron orbital is calculated by measuring the kinetic energy of the emitted electrons. The kinetic energies of the electrons are collected by using a detector and the binding energies are determined by this way. Thus the atomic composition of the sample is determined. Figure 4.6 shows the instrumentation of X-ray photoelectron spectroscopy.
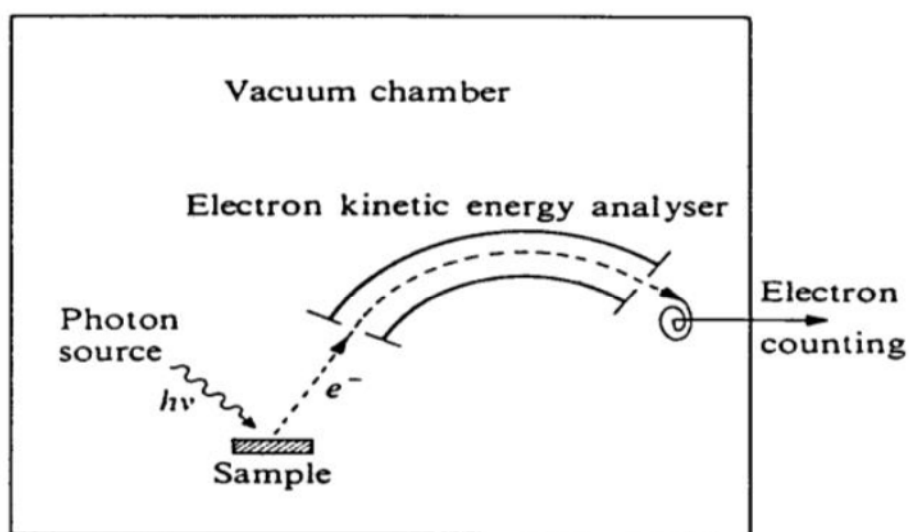
Figure 4.6. The instrumentation of X-ray photoelectron spectroscopy (XPS) [60]

After the photoemission process of the electron, XPS spectrum data is obtained as shown in Figure 4.7. An XPS spectrum consists of peaks corresponding to the binding energy of the photoelectrons. The electron binding energy peaks are investigated to determine the composition of the sample. The integrated intensity of an XPS spectrum is proportional to the density of atoms in the sample. The photoelectron lines in alloy material are much complicated than homogeneous samples [62].
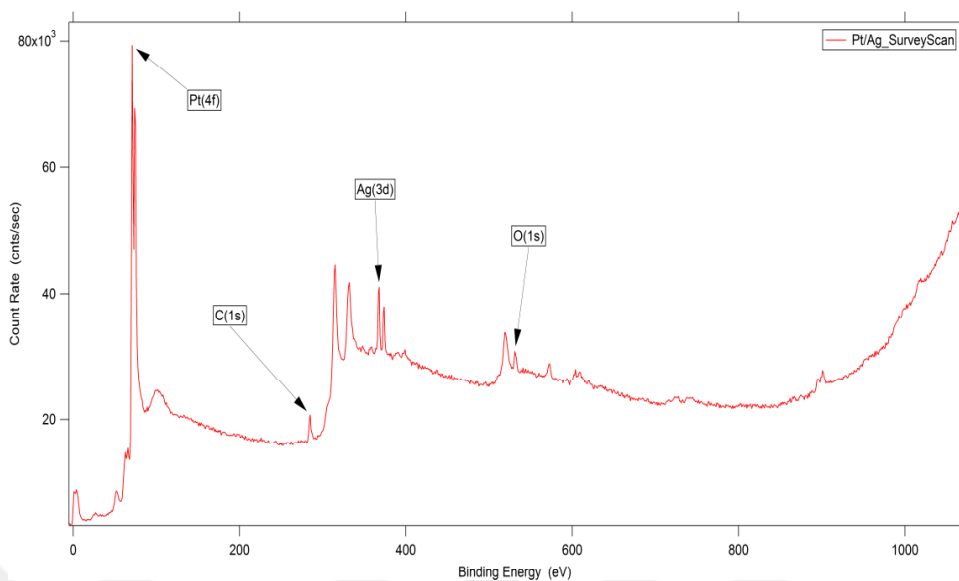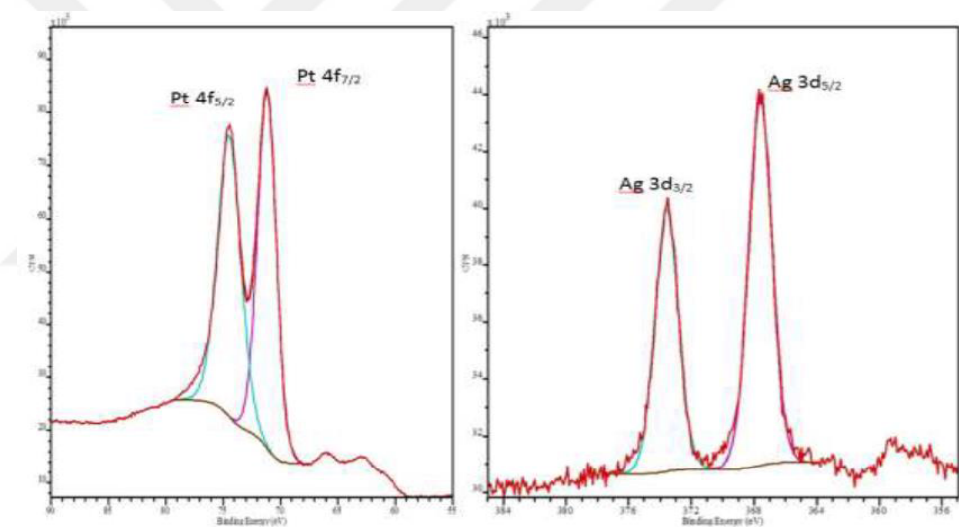
Figure 4.7. (a) Survey scan spectrum, (b) Pt 4f narrow scan XPS spectrum, (c) Ag 3d narrow scan XPS spectrum of PtAg film

The measurement of the peak area aids to detect the composition of the material surface. The composition of the sample surface is determined by taking the ratio of the area under the binding energy curve for each element in the measured sample. The area under the binding energy curve in the spectrum is proportional to the number of atoms that emit the electrons at that binding energy.

4.2.2. X-ray diffraction technique (XRD)

X-ray diffraction (XRD) is a technique which is used to identify the crystal structure of materials such as films, bulk and powders. Orientation of the crystal, unit cell dimension, grain size, phase composition and defect structures of the materials are determined by using XRD technique.

XRD technique is based on the scattering of X-ray on a crystalline material. X- ray beam is pass through the crystalline material. The incident beam is scattered and diffracted into many specific directions. The beams produce many diffraction patterns which consist of the dark spot points having different intensities on a photographic film plate as shown in Figure 4.8. The scattered rays contribute to obtain information about the structures of crystalline substances [63].
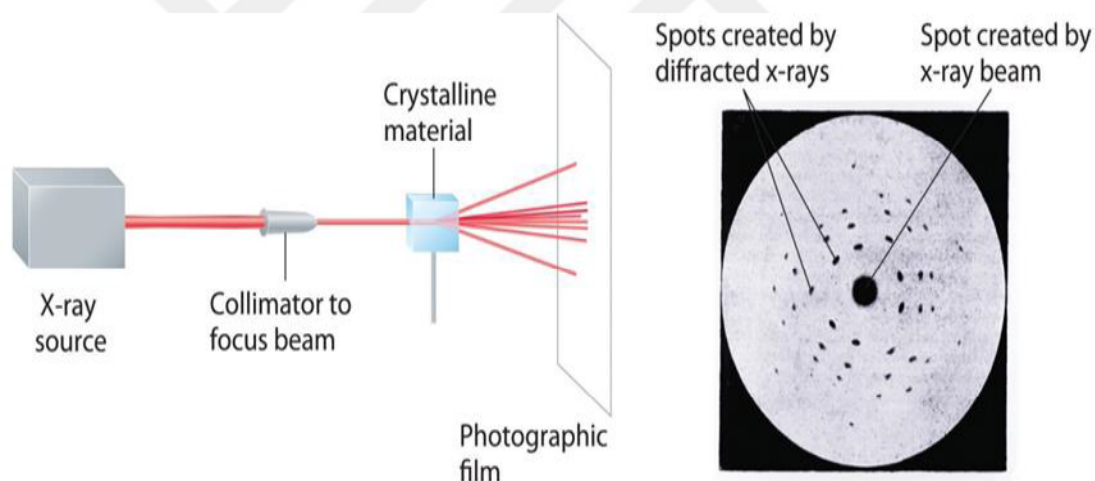
Figure 4.8. X-ray diffraction and diffraction pattern captured on a photographic film [63]

The theory of the XRD is explained by Bragg's law. The law explains why the cleavage faces of the crystals appear to reflect X-ray beams at specific wavelengths and the incident angles [64].

Bragg's law is used to measure the interlayer spacing which refers to the distance between two parallel planes of atoms in a crystalline material. The interplanar distance contributes to determine the dimensions of the unit cells.

The atoms in the crystalline solids are typically arranged in planes. Bragg's law illustrates that the atoms are arranged as parallel planes in the crystal and each plane of the atoms in a crystal acts as a reflecting surface. When X-ray beams interact with the components of a crystalline lattice with an angle of θ, they are scattered by the electrons of atom at the same angle. The reflection of X-rays from two parallel planes of atoms causes an occurence of the constructive interference of X-rays. If two X-ray beams strike a lattice of atoms, the waves are scattered from the two planes sepatared by the interplanar distance, d. This means that the wavelength of the beam and thus the peaks in the X-ray diffraction pattern are directly related to the interatomic distances in the crystal.

The relationship between X-ray wavelength and the interatomic distance is described as Bragg equation, as shown in Equation 4.2.

$$2d \sin \theta = n\lambda \tag{4.2}$$

In the equation, d is the spacing between the layers of atoms, θ is the angle between X-ray and the planes in the crystal, λ is the wavelength of the X-ray beam and n is any integer representing the order of the diffraction peak.

The lower X-ray beam hits the atom in the lattice travel extra distance by $2d\sin\theta$ when it is compared to the upper beam shown in Figure 4.9. The extra distance should be an integral multiple n of the wavelength so that the beams arrive at the detector in a diffractometer.
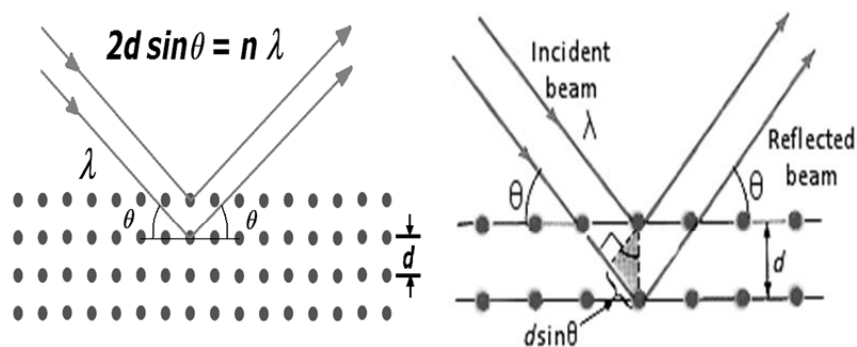
Figure 4.9. The working principle of X-ray diffraction [65, 66]

The interplanar distance between the atoms is a characteristic property. Each solid material has different interatomic distance. This means that X-ray beams are diffracted at a different angle θ. By measuring the angles and intensities of the diffracted beams, materials can be analyzed by using XRD technique.

4.2.3. Four probe method

Four-point probe method is one of the most commonly used electrical characterization technique for measurement resistivity of materials which is thin film or bulk sample. Four point technique is an effective, simple and reliable method for resistivity measurements. Resistivity is one of the important electrical parameter and it is directly related to the impurity of a sample. The method is used to characterize material by measuring its resistivity.

The experimental set-up consists of four probes are arranged linearly on the material surface. The probes are aligned in a straight line at equal distance from each other. In the system, a constant current (I) is applied in the two outer probes and the voltage (V) drop is measured in the inner probes. The values of the sourced current and the measured voltage are used to determine the sample resistivity of the shallow layers. Figure 4.10 shows the arrangement of four probes on the surface.
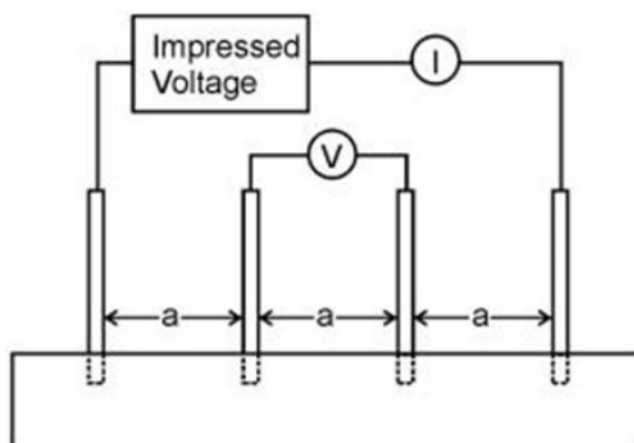
Figure 4.10. Schematic four-point probe configuration on a sample [67]

Four probe method is used for detecting the sensor characterization instead of two point set-up. In the two point set-up, current and voltage are measured in the same wire. The measured resistivity is the sum of the resistivity in the material and the resistivity in the contact point between the sample and electrode. Therefore it is difficult to separate the sample resistance from the contact resistance. For high resistivity measurement, two probe method can be used because the contact resistance between the sample and the electrode is small and negligible. However for low resistivity, two point probing is not proper due to the contact effect is large and close to the sample resistance. Thus the contact resistances influence the results highly. In order to overcome the problem of the contact resistances for low resistivity, four probe configuration is used. Four electrode system is used to eliminate the measurement errors due to the contact resistance. It is the best method for materials having low resistivity [68]. The set up difference between two point probing and four point probing is illustrated in Figure 4.11.

Figure 4.11. The set-up comparison of the two probe and four probe system [69]

In the two point system, the probe contact resistances are R_1 and R_2 as shown in the Figure 4.11. The contact resistances which are caused from the contact points, R_1 and R_2 affect the measurement results. However in the four point system, the potential can be measured across the probes which do not carry any current. Because of high input impedance voltmeter, the inner probes in the circuit draw no current. The measurement is independent of the voltage probe resistances, R_1 and R_2. Thus voltage drop at the inner probe points is eliminated from the potential measurements.

There are some assumptions for detecting the resistivity of a sample. For a bulk sample where the thickness (t) of the material is much larger than the distance (s) between the probes, the electrical resistivity (ρ) of the sample is calculated with the help of the Equation 4.3.

$$\rho = 2\pi \times s \times \frac{V}{I}$$
(4.3)

In the equation; V is the voltage between the internal contact electrodes, I is the current between the outer probes and s is the spacing between two point electrode. In case of thin film, thickness (t) is much smaller than the distance (s) between the electrodes, the resistivity of the thin film is obtained by the Equation 4.4.

$$\rho = \frac{\pi}{\ln 2} \times \frac{V}{I} \times t$$
(4.4)

In the expression; V is the drop potential measured among the inner electrodes, I is the source current and t is the film thickness.

4.2.4. Gas sensor measurement system

There are several parameters such as sensitivity, selectivity, reversibility and the electronic parameters to evaluate the performance of gas sensing material. All these parameters are important for understanding the gas sensing mechanism of the sensor. The gas detection system supplies several basic informations about the gas sensing behaviour of the sensor.

Gas sensor measurement system is used to characterize the performance of the fabricated sensor. The test system is adjusted for all the conditions that are essential for the behaviour of the sensor. Thus it is possible to get information about the sensor properties and sensor behaviour. The gas sensing tests are carried out under the influence of certain target gases. The test is necessary for the understanding, development and optimization of the sensor.

When a sensing material is exposed to a target gas, it interacts with the gas molecules. The interaction between the sensing material film and the gas which is called adsorption-desorption process causes the chemical reactions that occur on the surface or bulk of the material. This interaction changes some properties of the sensing material, such as the electrical conductivity or the mass. The conductivity change is detected by the voltage drop over a series resistor. The change in mass is detected by the shift in frequency of a resonator [40]. A schematic representation of the gas sensing test system is shown in Figure 4.12.
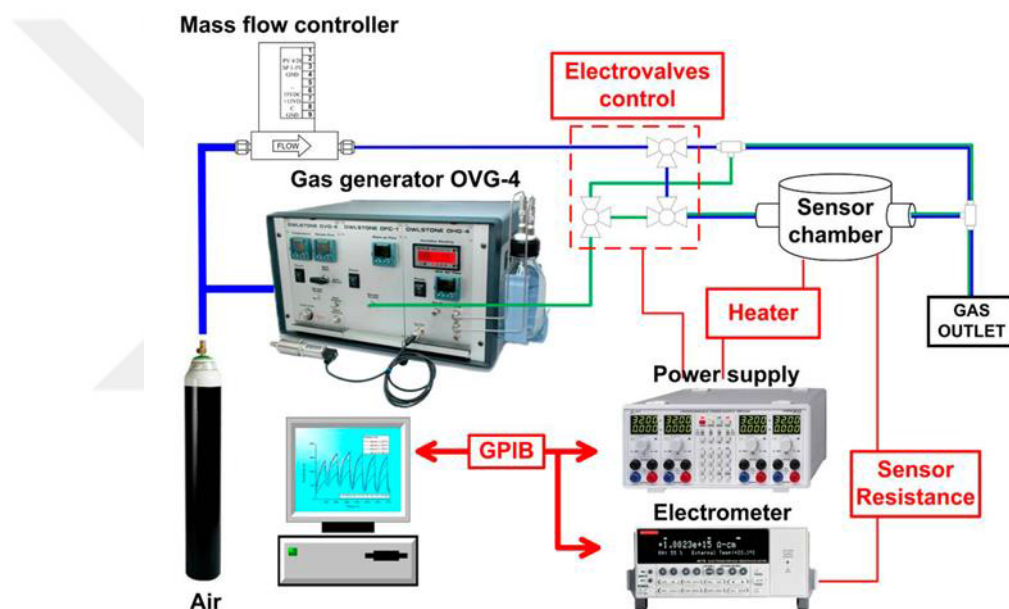
Figure 4.12. Schematic representation of the sensor test system [70]

The measurement system simply consists of sensor chamber, mass flow controller, temperature controller and electrometer. Gas sensor characteristics and electronic parameters of the sensor are measured using the designed sensor setup. The gas sensitivity of the sensor for different gases is investigated with the help of the detection setup. When the test gas comes into the chamber, the resistance change of the sensor is measured using the computer controlled electrometer. The resistance response of the sensor is also evaluated by changing the concentration of the gas. The concentration of the gas is adjusted by the mass flow meter array linked to the

multichannel gas flow controller unit. Besides, the sensing capability of the sensor is characterized at different operating temperatures with a precisely controlled heater inside the system, thus the optimum working temperature of the sensor is find out.

CHAPTER 5. PREPARATION OF SAMPLES AND EXPERIMENTAL SETUP

In this work, Pt and Pt-Ag alloy thin films were fabricated by sputter deposition technique. Structural and electrical characterization of the films were analyzed. The gas sensing properties of Pt and Pt-Ag alloy films were investigated.

5.1. Film Deposition Materials

5.1.1. Platinum

Platinum is an alternative sputtering metal for hydrogen gas sensor because of its promising properties. It is stable metal and melting point is 1772 ºC. Pt is one of the chemical catalyst and having good working performance for hydrogen detection [34]. Platinum is very unreacted metal and shows high resistance to corrosion even at elevated temperatures. Besides the resistance to oxidation of Platinum is quite better than Palladium metal.

5.1.2. Silver

Silver is another coating material for hydrogen gas sensor. Silver metal has the highest contact resistance, electrical conductivity and thermal conductivity in all elements in nature. Silver metallic thin film has face-centered cubic (FCC) structure and have highest packing density thus they show (111) planes. In addition to these properties, silver has low cost, ductility and no damage on human skin [42].

Table 5.1. Some properties of silver metal [42]

Bulk Resistivity (μ.cm) at 200 °C	Mean Free Path of Electron (nm)	Thermal Conductivity (W/m.K)	Melting Point (°C)
1.59	52	425	961

5.2. Pt-Ag Alloy Films

PtAg alloy films have been used to increase the sensitivity of hydrogen gas sensor. Silver has strong surface plasmon resonance (SPR) property and Ag is one of the widely used metal for sensor applications. In this study, the different chemical combinations of Pt and Ag in PtAg alloy thin films were created to understand the exact sensing mechanism of the metallic based- hydrogen sensor [71].

5.3. Preparation Of Pt Films

Prior to film deposition by sputtering system, the substrates were initially cleaned with acetone, isopropyl alcohol and high purity water in an ultrasonic cleaner.

The Pt thin films with different thickness were prepared using Radio Frequency (RF) sputtering method on microscope glass slide. The thin films were coated with a constant RF power at 5 mTorr argon (Ar) pressure during deposition by using a NANOVAK 400 PVD system as shown in Figure 5.1. The glass substrates were rotated with 10 rpm during Pt deposition and the film thickness were varied from 2 nm to 50 nm that was monitored in situ during the deposition via a QCM from Inficon.

Figure 5.1. Magnetron sputter system at Nıgde University

5.4. Deposition Of PtAg Thin Films

The Pt_xAg_{1-x} thin films were grown on a miscoscope glass slide by using co-sputtering technique. Co-sputtering has the advantage of easy tuning and also it allows to control the percentages of Pt and Ag in the film. In the sputter system, high purity Pt (99.999 %) and high purity Ag (99.999 %) were served as a target source materials. PtAg films were co-sputtered on the glass surface under 10^{-6} mbar high vacuum ambient. Two power supplies were used to deposit the thin films in the sputter chamber at the same time. RF power supply was used for Pt sputtering, the Ag sputtering was carried out with DC power supply. Sputtering process was carried on at 5 mTorr of pure Argon ambient to form a Pt_xAg_{1-x} thin film. 3 nm PtAg films with different composition ratios were fabricated. The chemical compositions were adjusted as $Pt_{0.95}Ag_{0.05}$, $Pt_{0.90}Ag_{0.10}$, $Pt_{0.80}Ag_{0.20}$ and $Pt_{0.50}Ag_{0.50}$.

5.5. Structural Characterization Of Pt And PtAg Thin Films

The morphologies of Pt thin films were studied by Scanning Electron Microscopy (SEM, ZEISS EVO LS15). The crystal structures of one of Pt films were examined by X-ray diffraction (Rigaku Smartlab diffractometer) by using Cu Kα= 0.15418 nm radiation in the angle range of $30° - 90°$. XPS measurements of Pt thin film were performed by using a Thermo 10 Scientific K-Alpha X-ray photoelectron spectrometer with monochromatic Al Kα radiation (1486.3 eV) as a X-ray source.

5.6. Gas Sensor Measurements Of Pt And PtAg Thin Films

All the fabricated Pt and PtAg thin films were tested by hydrogen gas mixture. Figure 5.2 illustrates the experimental setup for fabrication of Pt film deposition. Four Au pad electrodes were contacted on the top of Pt and PtAg thin films for H_2 gas sensing measurements as shown in Figure 5.3. The changes of resistance for each film were recorded via a four point-probe connected to a multimeter (Agilent34410A).

Glass slide substrate   **Pt thin film layer deposited by sputtering**   **Four point conductance electrodes onto the Pt surface**
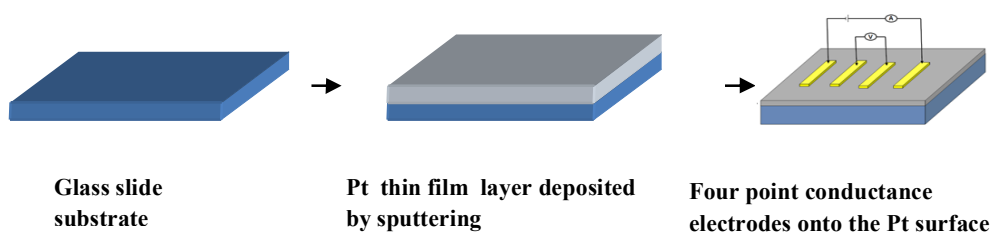
Figure 5.2. Experimental process of hydrogen sensor fabrication in three steps
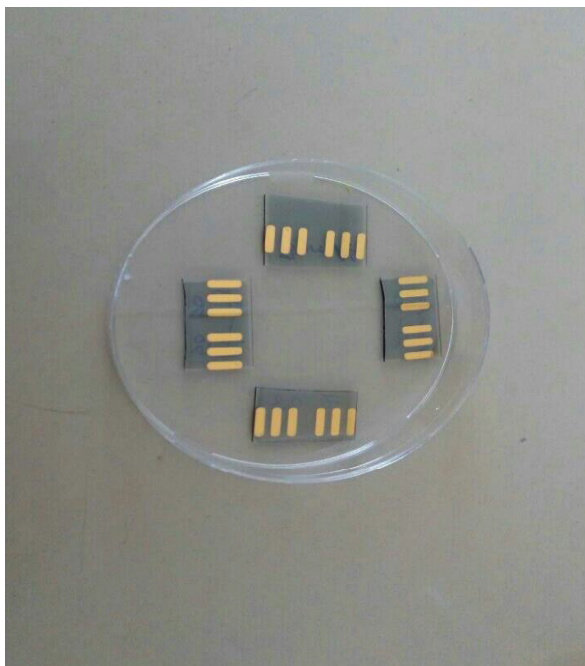
Figure 5.3. Four Au pad electrons on the top of Pt and PtAg films

The H_2 gas sensor measurement systems were composed of a flow-type aluminum measurement chamber including a heatable sample holder, a mass flow control unit (MKS), a temperature controller (Lakeshore 340), a multimeter and gas measurement chamber. A gas chamber and mass flow meters are shown in Figure 5.4 and Figure 5.5.
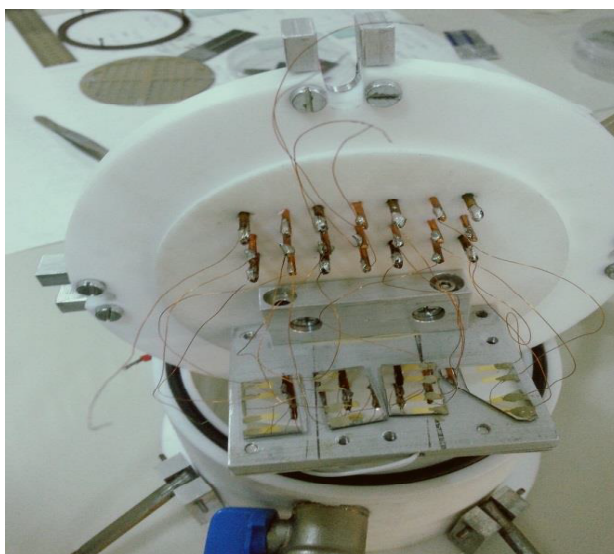
Figure 5.4. Image of gas measurement chamber

The concentrations of H_2 in high purity dry air were varied from 1000 ppm (0.1 %) to 50000 ppm (5 %). The volume of the measurement chamber was 1 liter and a constant total gas flow rate of 200 sccm was applied. Resistance-time (R-t) characteristics for investigating gas sensing properties of Pt and Pt-Ag thin film sensors were measured by changing atmospheric conditions in the measurement cell in situ at various temperatures (from 30 ºC to 200 °C). All measurements data were recorded using an IEEE 488 data acquisition system incorporated to a personal computer. The percentage sensitivity % is generally defined as shown in the Equation 5.1.

$$S = \frac{R_0 - R_g}{R_g} \; x \; 100 \tag{5.1}$$

R_g is the resistance after the sensor is exposed to the H_2, and R_0 is the reference value (baseline resistance) of the sensor exposed to high-purity dry air.

Figure 5.5. Mass flow meters used for regulating gas flow into the measurement cell

CHAPTER 6. RESULTS AND DISCUSSIONS

6.1. Structural Characterization Of Pt Thin Films

SEM images of Pt thin films with different thickness (2 nm: Figure 6.1a, 5 nm: Figure 6.1b and 15 nm: Figure 6.1c) are given in figure 6.1. All Pt thin films are homogeneously covered on the glass surface. The surfaces of the samples seem to be quite smooth as seen in Figure 6.1. Increasing the thickness of Pt thin film, a film formation on the surface was clearly observed.
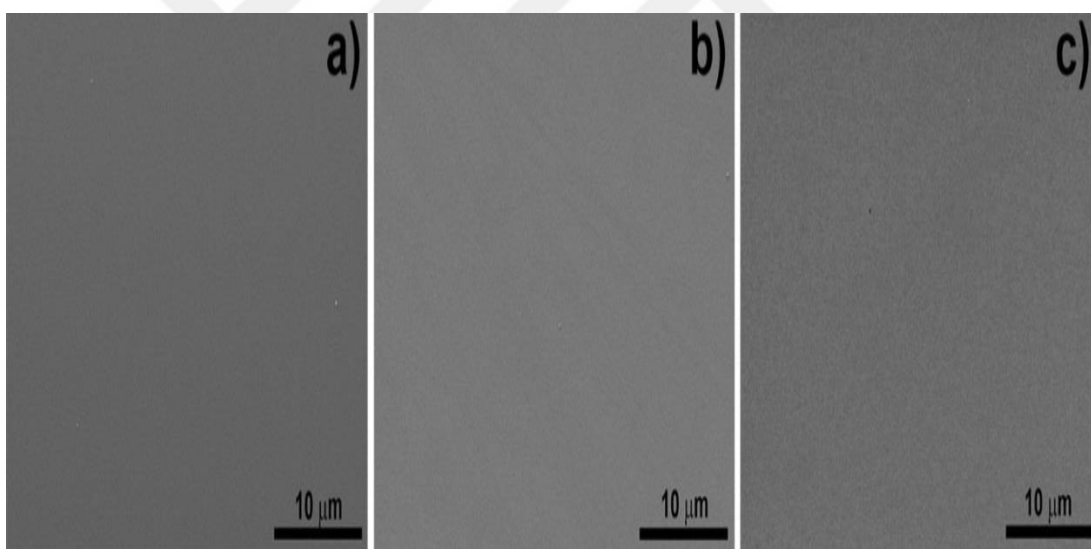
Figure 6.1. SEM images of Pt thin films with the thickness of (a) 2 nm, (b) 5 nm, (c) 15 nm

The XRD and EDX patterns for the Pt thin films are displayed in Figure 6.2. In figure 6.2 (a), the patterns show strong (111) and (200), and weak (200) and (131) reflections at 30.95°, 46.25°, 67.55° and 81.35° respectively and all of which correspond to a face-centered cubic (fcc) crystalline structure. The obtained thin film contain no impurity peaks, which is due to the high purity crystals and these results are well aggreement with previously published paper [72 - 75]. The EDX spectra for 5nm Pt thin film is shown in Figure 6.2 (b) and it is clearly seen Pt peak from the

spectra. The other peaks belong to oxygen (O), silicon (Si), sodium (Na), magnesium (Mg) and aluminum (Al) were observed representing the glass substrate. The atomic percentage of Pt on the glass substrate increased by increments of the thickness of Pt thin films. As well as other analysis techniques, X-ray photoelectron spectroscopy (XPS) was used to check the film purity. Figure 6.2 (c) shows the high resolution window XPS spectra for the major photoemission Pt 4f core level region. The peaks positions of Pt $4f_{7/2}$ and $4f_{5/2}$ were about 71.1 eV and 74.5 eV correspond to pure Pt metallic state [76 - 78]. We did not observe oxygen and other different elements from wide scan XPS spectrum.
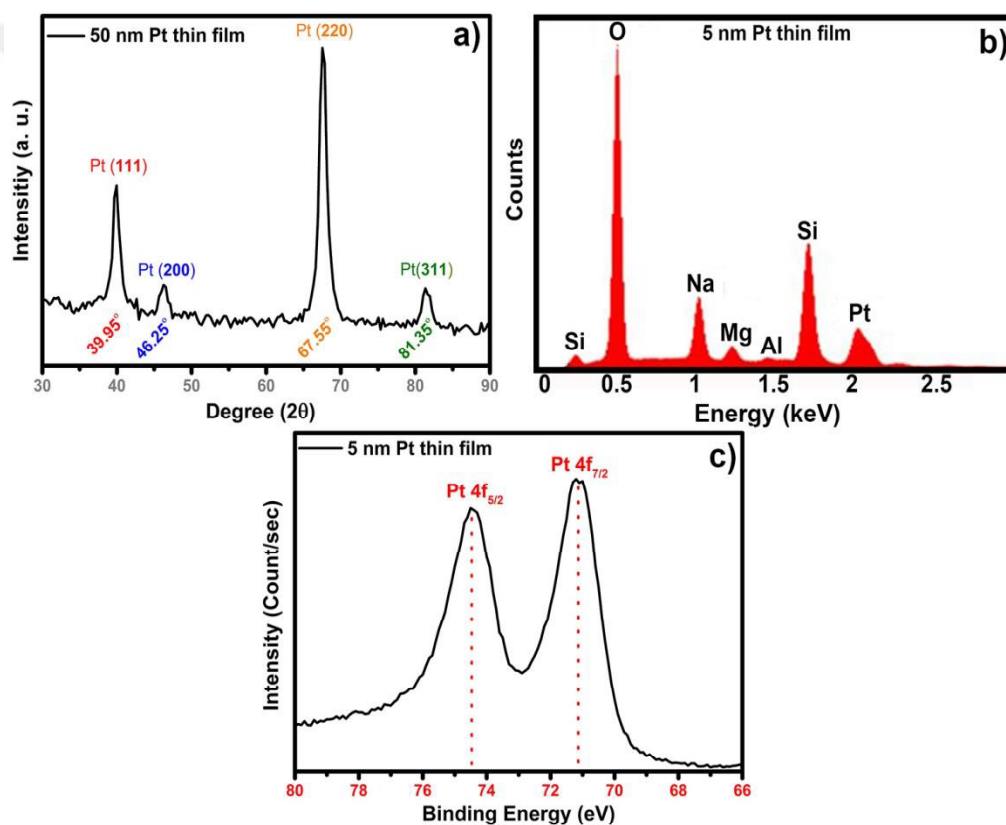

Figure 6.2. (a) XRD patterns for 50 nm Pt thin film, (b) EDX graphs for 5 nm Pt thin film and (c) XPS spectra of Pt 4f for 5 nm Pt thin film

6.2. Gas Sensing Measurements Of Pt Films

The resistances of Pt thin films were investigated under a dry air flow at the temperature range from 30 °C to 200 °C. The resistances of the Pt thin films

depending on temperature are given in Figure 6.3. Temperature dependent changes of the resistances for 2 nm Pt and 5 nm Pt thin films were linearly increased throughout the entire measured temperature interval from 30 °C to 200 °C due to the its metalic structure. Besides, it was clearly observed that the resistances of the Pt thin films were inversely proportional to the thickness of thin films, which is compatible with the equation of $R = P\dfrac{l}{A}$ given for resistance of a conductor.

In the equation; R is resistance, ρ is resistivity, l is length and A is area.
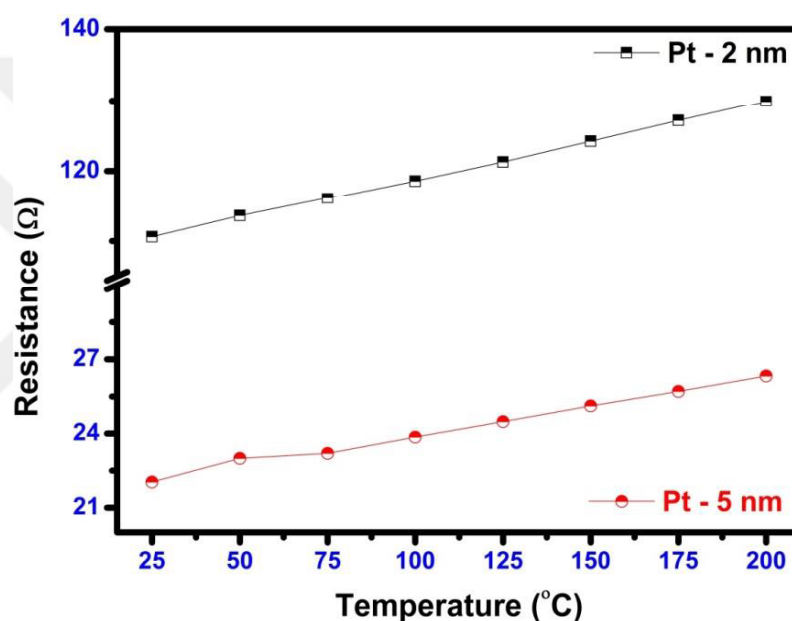
Figure 6.3. Temperature dependent resistance values for 2 nm and 5 nm Pt thin films

The H_2 sensing properties of Pt thin film devices were investigated at different temperatures as seen in Figure 6.4. The resistance versus time graph of the 2 nm and 5nm Pt thin film sensors under 1000 ppm H_2 at 30 °C the indicated temperatures are given in Figure 6.4a and 6.4b. After exposure to 1000 ppm H_2, the resistance of both 2 nm and 5 nm Pt thin film sensors decreased and then, the rate of decline reached saturation for all measured temperatures. After the measurement chamber was cleaned with dry air, the resistance of the sensors increased rapidly and then come to saturation. The base line of both 2 nm and 5 nm Pt thin film sensors are shifted at 30 °C and at 100 °C. But, the both sensors are fully reversible above the temperature of 100 °C as seen in Figure 6.4a and Figure 6.4b. It is clearly seen for both Pt thin film

sensors that the base line resistances of the sensors increased with enhancing the temperature such as mentioned in Figure 6.4. Also, if it is looked at the time scale bar carefully, the time scale is not same at different temperatures for the both sensors. Previously, Patel et al. deposited thin nanoparticulate Pt films with a nominal thickness of 35 Å on SiO_2 by using electron beam evaporation, and investigated the structure and H_2 response of the film depending on temperature and H_2 concentration (10-1000 ppm) [39]. They reported that exposure to ppm level of H_2 in the presence of 5 % oxygen with nitrogen as the carrier gas caused decreases in electrical resistance and the sensitivity of the film became more pronounced with increasing temperature, indicating that the response mechanism for H_2 sensing was an activated process. Yang et al. prepared Pd and Pt nanowires using lithographically patterned nanowire electrodeposition and reported the performance of a single Pt nanowire for detecting H_2 in air comparison with Pd nanowire [37]. Yoo et. al fabricated Pt nanowire arrays using advanced lithographic techniques with a small cross sectional dimension $(10 - 40$ nm), investigated H_2 gas sensing properties of the nanowires and explained the sensing mechanism with reduced electron scattering in the cross section of the hydrogen adsorbed Pt nanowires [79].

In our case, the sensing mechanism of Pt thin films could be explained as follow; Pt does not form a bulk hydride phase upon exposure to H_2 such as Pd [37, 39, 79]. A schematic diagram for hydrogen sensing mechanism is given in Figure 6.4c. The surface of Pt thin film covered with the absorbed oxygen atoms under dry air (Figure 6.4 c-1). While the hydrogen exposed to Pt thin film, hydrogen atoms start to displace oxygen on the Pt surface (Figure 6.4 c-2 and Figure 6.4 c-3). After whole surface of Pt thin film covered with hydrogen, the number of charge carrier scattering at the Pt surface decreases. So, the decrease in the resistance of Pt thin film when exposed hydrogen could be related to decreasing the number of the surface charge carrier scattering. The ad/absorbsoption and desorption of hydrogen and oxygen in dry air from Pt thin film surface could be explained with following reactions, 6.1, 6.2 and 6.3 [80 - 82].

$$Pt + \frac{1}{2}O_2 \rightarrow Pt-O \qquad\qquad (6.1)$$

$$Pt-O + \frac{3}{2}H_2 \rightarrow Pt-H + H_2O \qquad (6.2)$$

$$2Pt-H + \frac{3}{2}O_2 \rightarrow 2Pt-O + H_2O \qquad (6.3)$$

When the molecular oxygen reacts with Pt surface in dry air condition, chemisorbed oxygen atoms form as seen in Reaction 6.1. If Pt surface atmosphere condition changes from dry air to molecular hydrogen, hydrogen atoms displace oxygen atoms on the Pt surface with catalytic formation of water and its desorption from the Pt surface as presented in Reaction 6.2. While the chemisorbed hydrogen atoms on Pt surface is react with dry air condition, oxygen atoms replace hydrogen atoms on the Pt surface with water formation as seen in Reaction 6.3. The replacement of the surface atoms (hydrogen or oxygen) is a reversible process.
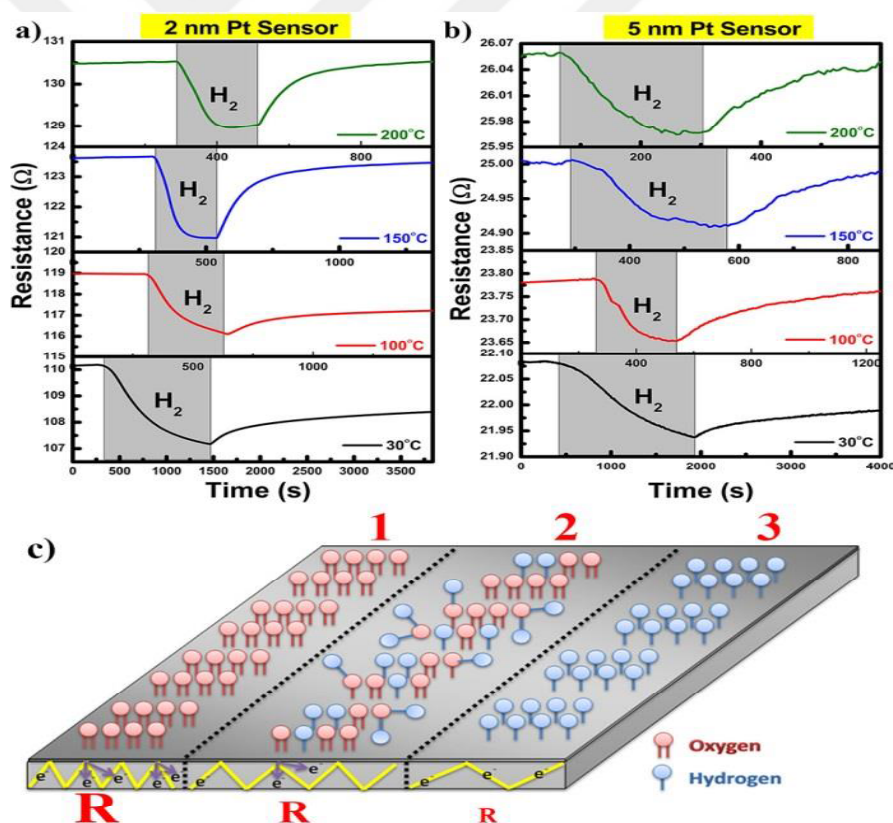

Figure 6.4. The resistance versus time graph for 2 nm (a) and 5 nm (b) Pt thin films exposed to 1000 ppm H_2 at indicated temperatures. (c) A schematic diagram for H_2 ad/absorbtion on Pt surface

Temperature dependent sensitivities for 2 nm and 5 nm Pt thin film sensors against 1000 ppm H_2 were given in Figure 6.5a. The sensitivites of 2 nm and 5 nm Pt thin film sensors decreased from 2.7 and 0.7 to 1.1 and 0.3 with increasing temperature respectively. The sensitivities of 2 nm Pt thin film sensor are higher than the sensitivities of 5 nm Pt thin film sensor for the measured temperature interval as seen in figure 6.5a. So, the sensitivities of Pt thin films for H_2 is strongly affected by the thickness of Pt film. Similarly, this behavior have been observed for Pt nanowire with different dimentions [37, 79]. The response time (t_{90}) is defined as the times required for the change in the resistance variation level of 90% upon initiating the desired H_2 concentration. Figure 6.5b shows the response time as a function of temperature for both 2 nm and 5 nm Pt thin film sensors. The response time of 2 nm Pt thin film sensors is lower than that of 5 nm Pt thin film sensor at room temperature and this behavior could be explained with a short diffusion path. However, above the temperature of 100 °C the response time of the both sensors is approximately the same as shown in Figure 6.5b. The response time is also decreased with increasing temperature for the both sensors and this behavior can be explained with a faster diffusion of hydrogen at higher temperatures.
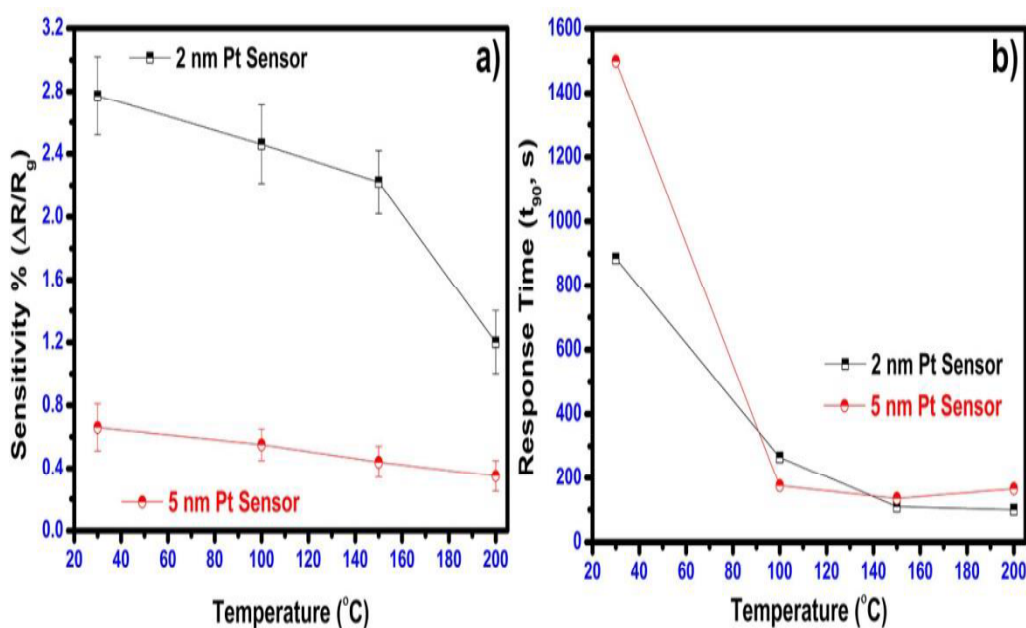

Figure 6.5. Temperature dependent sensitivities (a) and response time versus temperature (b) for both 2 nm and 5 nm Pt thin film sensors exposed to 1000 ppm H_2

In order to investigate concentration dependent H_2 sensing properties, a measurement were performed at 150 °C for 2 nm Pt film sensor due to fully reversible and recovery properties that observed for 1000 ppm H_2 exposure. The resistance versus time for 2 nm Pt film sensor at 150 °C exposed to H_2 concentration interval of 0.1 %-1 % is shown in Figure 6.6a. After exposure to every desired H_2 concentration, the resistance of 2 nm Pt thin film sensors decreased, the rate of decline reached saturation and then after cleaning with dry air, the resistance of the sensor increased rapidly to its base line. The change in the resistance is enhanced with increasing H_2 concentration as seen in Figure 6.6a. The sensitivity versus the concentration for 2 nm Pt thin film sensor at 150 °C is shown in Figure 6.6b. The dependence of the sensitivity on the H_2 concentration was nearly linear at low concentrations, and the sensitivity started to a decrease tendency for high concentrations above 1 % H_2. The sensitivity % increased from 0.8 to 10.2 between 0.1 % H_2 and 5 % H_2.
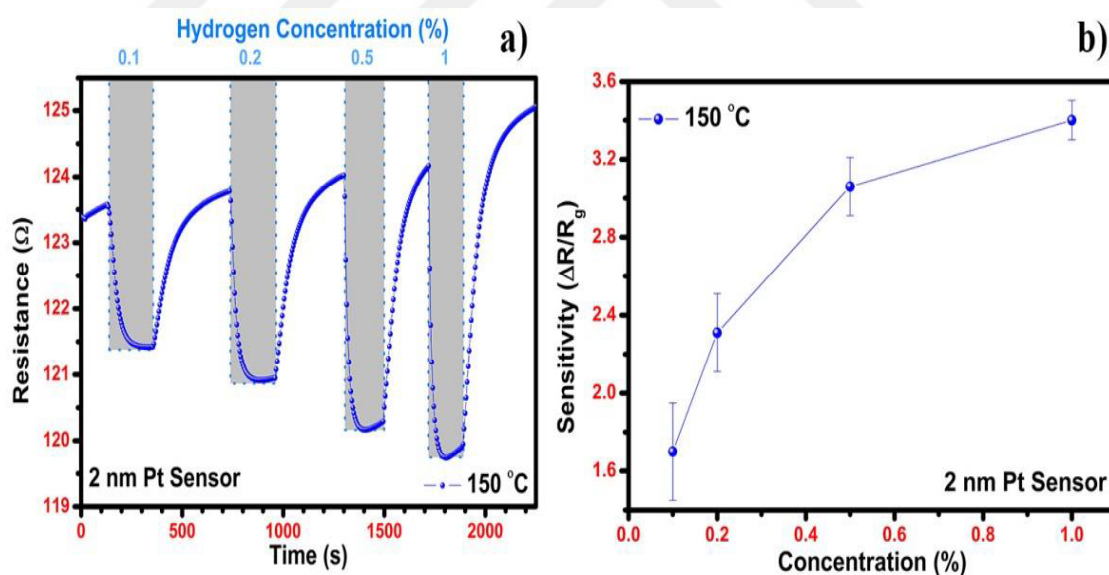
Figure 6.6. The resistance versus time graph (a) and H_2 concentration dependent the sensitivity graph (b) for 2 nm Pt thin film sensor at 150 °C

6.3. Structural Characterization Of PtAg Films

PtAg films were investigated by using energy dispersive spectroscopy (EDX). Figure 6.7 shows EDX results for PtAg thin films with different chemical compositions. Pt and Ag peaks are clearly seen from the EDX graph for each PtAg alloy film. Oxygen (O), silicon (Si), calcium (Ca), sodium (Na), magnesium (Mg) peaks are caused from the chemical composition of the glass substrate.
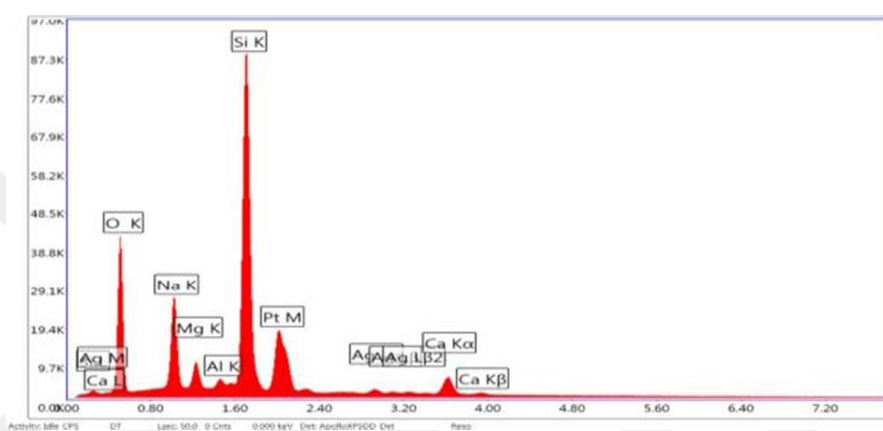
(a)
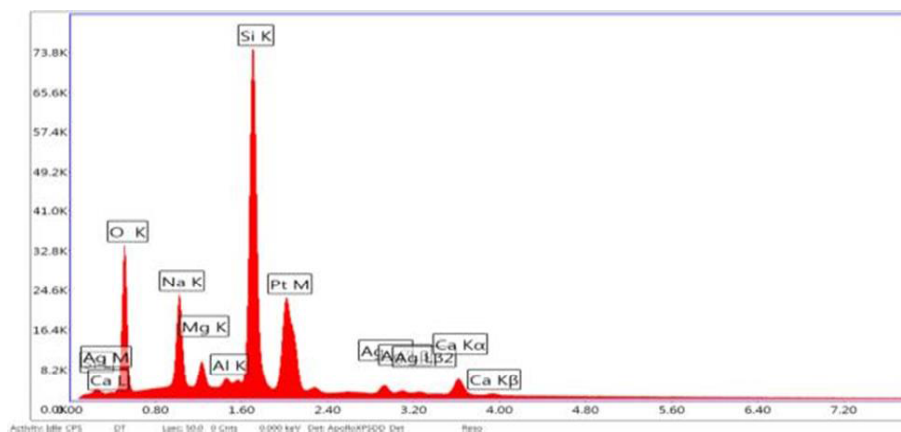
(b)
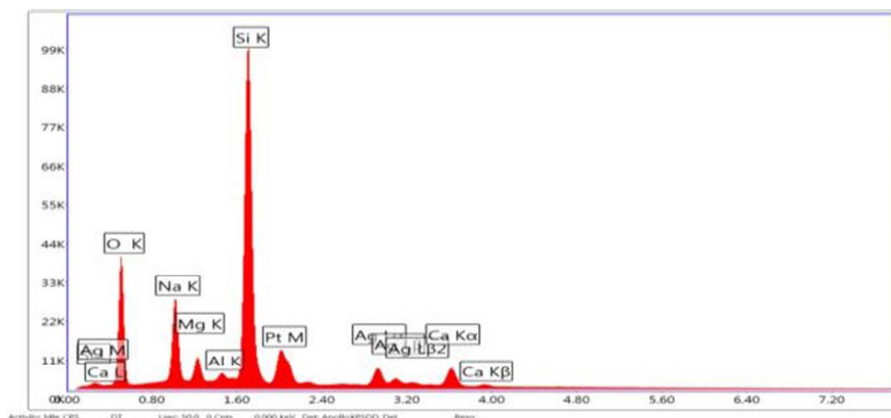
(c)

Figure 6.7. EDX graphs of (a) $Pt_{0.90}Ag_{0.10}$, (b) $Pt_{0.80}Ag_{0.20}$ and (c) $Pt_{0.50}Ag_{0.50}$ thin films

X-ray photoelectron spectroscopy (XPS) was used to check the purity of PtAg films. The XPS results are well agreement with EDX results in point of the chemical compositions of PtAg films. Figure 6.8 shows the XPS survey scan spectrum of $Pt_{0.90}Ag_{0.10}$ thin film. Figure 6.9 depicts the XPS spectra for the major photoemission Pt 4f and Ag 3d core level region. Also carbon and oxygen peaks are seen in the XPS spectrum. The other unnamed peaks are belong to Auger peaks of Pt and Ag.
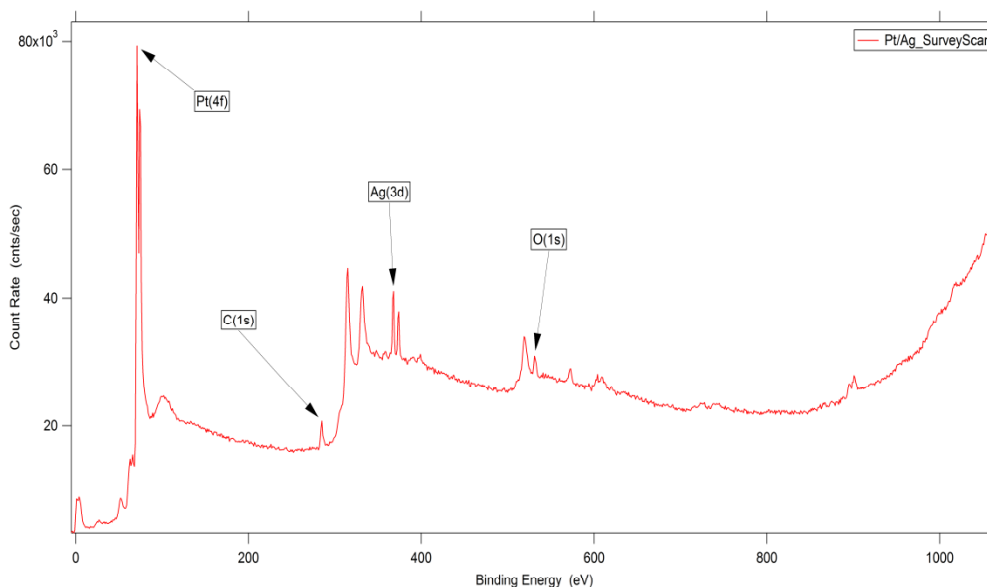
Figure 6.8. XPS survey scan spectrum of $Pt_{0.90}Ag_{0.10}$ thin film
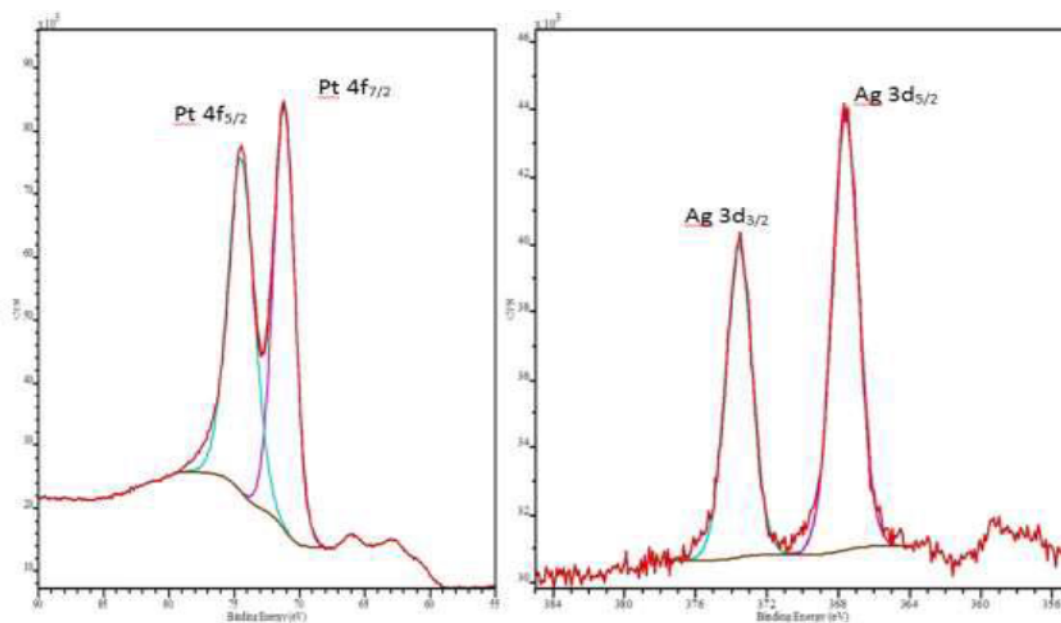
Figure 6.9. (a) Pt 4f narrow scan XPS spectrum, (b) Ag 3d narrow scan XPS spectrum of $Pt_{0.90}Ag_{0.10}$ film

The XRD spectrum of PtAg thin films are given in Figure 6.10. PtAg thin films were analyzed between 0° and 90° with the step of 0.05°. XRD peaks shifted toward the left side of the spectrum caused from the compositon of Ag in PtAg alloy increased from 10 % to 50 %.
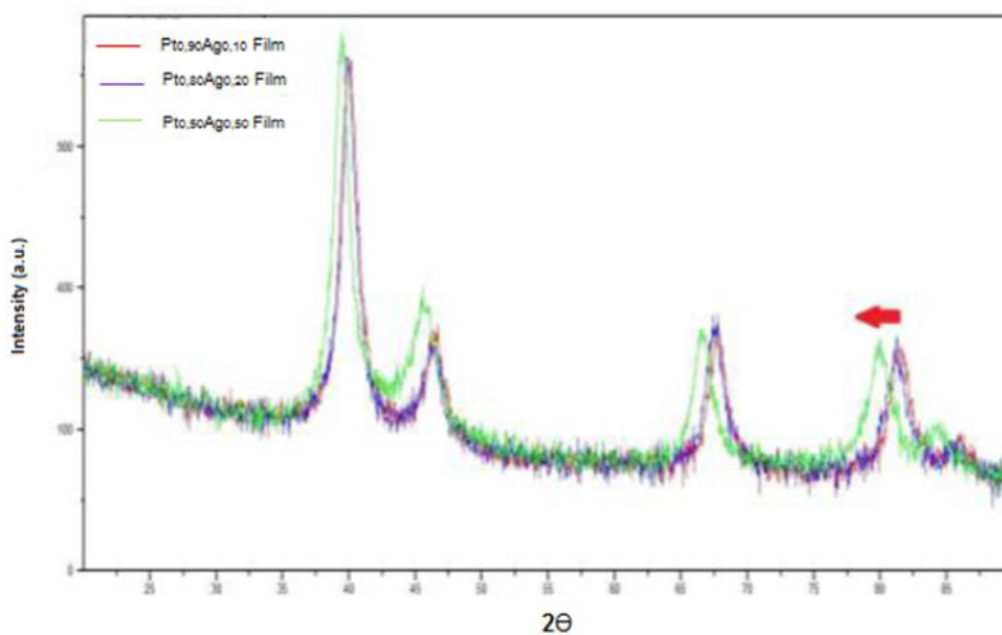
Figure 6.10. XRD patterns for Pt_xAg_{1-x} (x = 0.90, 0.80 and 0.50) thin films

6.4. Gas Sensor Measurements Of PtAg Films

The resistances of PtAg thin films were analyzed under dry air flow at the temperature range between 30 °C and 200 °C against 1000 ppm H_2. The resistances of the PtAg thin films depending on temperature are shown in Figure 6.11. The resistances of the sensors increased when the measured temperature increased. Temperature dependent changes of the resistances for 3 nm $Pt_{0.95}Ag_{0.05}$, $Pt_{0.90}Ag_{0.10}$ and $Pt_{0.80}Ag_{0.20}$ thin films were increased with enhancing the temperature from 30 °C to 200 °C.

Figure 6.11. Temperature dependent resistance values for 3 nm (a) $Pt_{0.95}Ag_{0.05}$ thin film(b) $Pt_{0.90}Ag_{0.10}$ thin film (c) $Pt_{0.80}Ag_{0.20}$ thin film

Temperature dependent sensitivites % for 3 nm $Pt_{0.95}Ag_{0.05}$, $Pt_{0.90}Ag_{0.10}$ and $Pt_{0.80}Ag_{0.20}$ thin film sensors under 1000 ppm H_2 are given in Figure 6.12. The sensitivities % of $Pt_{0.95}Ag_{0.05}$, $Pt_{0.90}Ag_{0.10}$ and $Pt_{0.80}Ag_{0.20}$ increased from 0.05, 0.04 and 0.03 to 0.11, 0.19 and 0.11 with increasing temperature, respectively. The sensitivity % of $Pt_{0.80}Ag_{0.20}$ thin film sensor is higher than the sensitivities of $Pt_{0.90}Ag_{0.10}$ and $Pt_{0.95}Ag_{0.05}$ sensors for the measured temperature from 30 °C to 200 °C as seen in Figure 6.12. This shows that the sensitivities of PtAg thin film sensors are affected from the chemical composition of the films for H_2 gas detection.
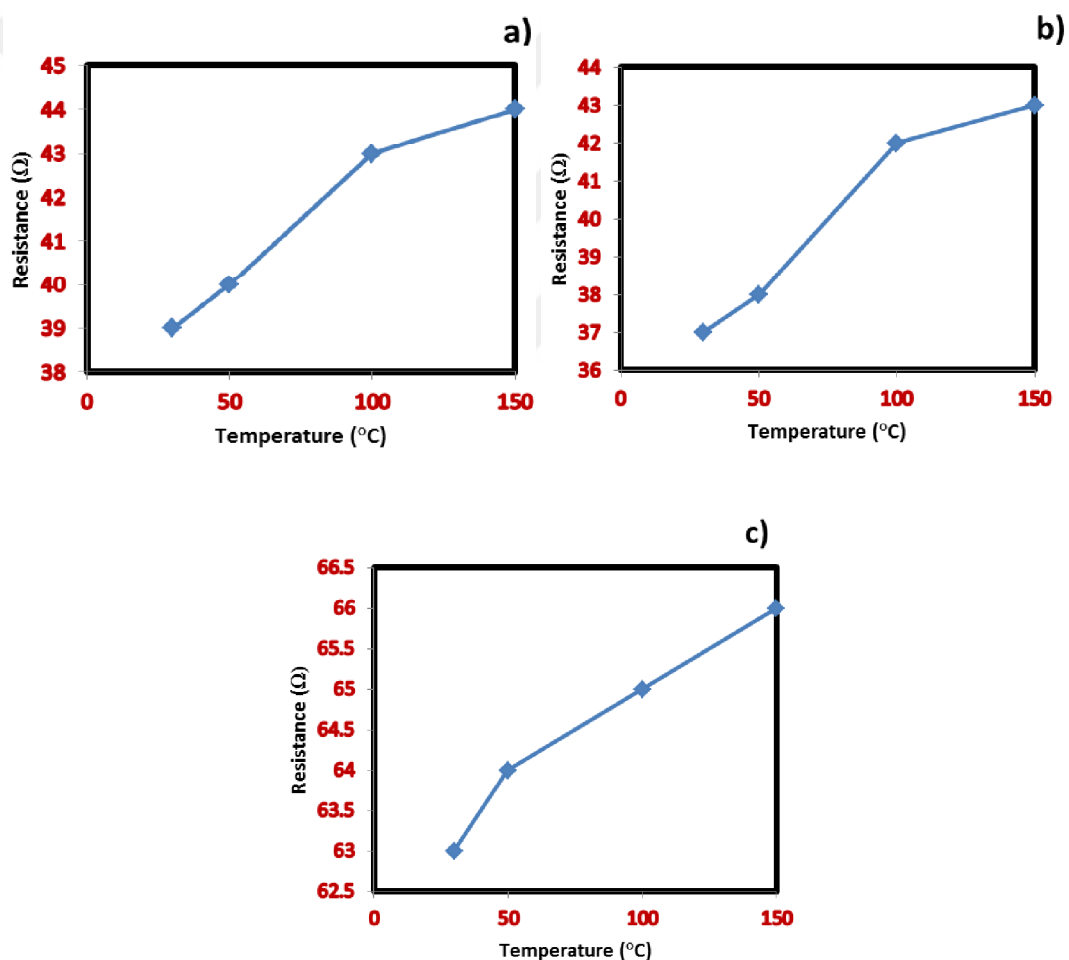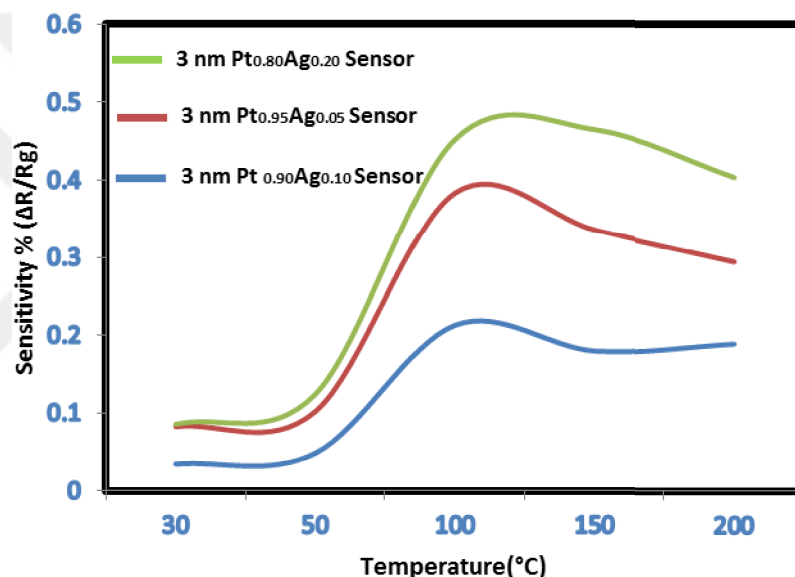

Figure 6.12. Temperature dependent sensitivities for 3 nm $Pt_{0.95}Ag_{0.05}$, $Pt_{0.90}Ag_{0.10}$ and $Pt_{0.80}Ag_{0.20}$ thin film sensors exposed to 1000 ppm H_2

Figure 6.13 shows the change in sensitivity with concentration of H_2. The sensitivity % changes of $Pt_{0.90}Ag_{0.10}$, $Pt_{0.95}Ag_{0.05}$ and $Pt_{0.80}Ag_{0.20}$ thin film sensors are given in Figure 6.13a and Figure 6.13b respectively. The sensitivity results of $Pt_{0.90}Ag_{0.10}$ thin film sensor are well agreement with the results for $Pt_{0.95}Ag_{0.05}$ sensor. The sensitivites % of $Pt_{0.90}Ag_{0.10}$ and $Pt_{0.95}Ag_{0.05}$ sensors increased linearly from 0.123 and 0.124 to 0.203 and 0.269 respectively until H_2 concentration reaches to 200 ppm. After 200 ppm H_2, the sensitivities % of both PtAg sensors started to decrease to 0.156 and

0.164. However the sensitivities of $Pt_{0.80}Ag_{0.20}$ sensor increased linearly with increasing hydrogen concentration. The sensitivity of $Pt_{0.80}Ag_{0.20}$ sensor increased from 0.02 to 0.362 with increasing H_2 concentration from 25 ppm to 1000 ppm as seen in Figure 6.13b.
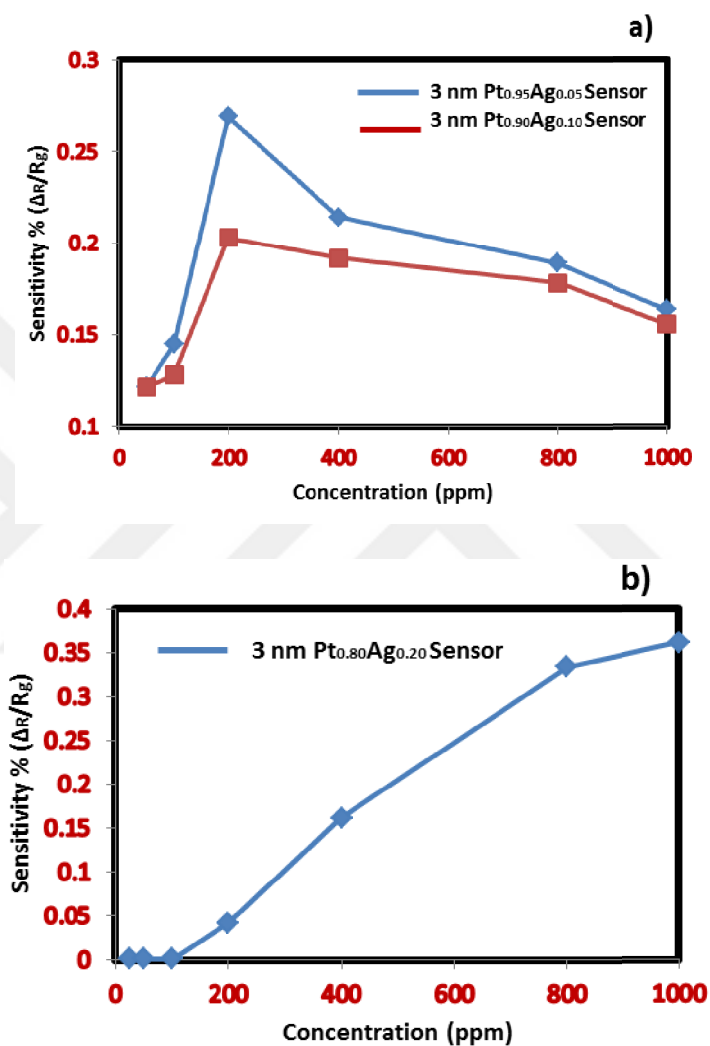
Figure 6.13. H_2 concentration dependent the sensitivity graph for (a) $Pt_{0.95}Ag_{0.05}$ and $Pt_{0.90}Ag_{0.10}$ sensors (b) $Pt_{0,80}Ag_{0,20}$ thin film sensors at 150 °C

$Pt_{0.80}Ag_{0.20}$ sensor has the best response time among the other PtAg thin film sensors. Figure 6.14 shows the response time (t_{90}) versus temperature for $Pt_{0.80}Ag_{0.20}$ sensor The response time decreased as the temperature increased for $Pt_{0.80}Ag_{0.20}$ sensor. The response time of $Pt_{0.80}Ag_{0.20}$ sensor is better at high temperatures.
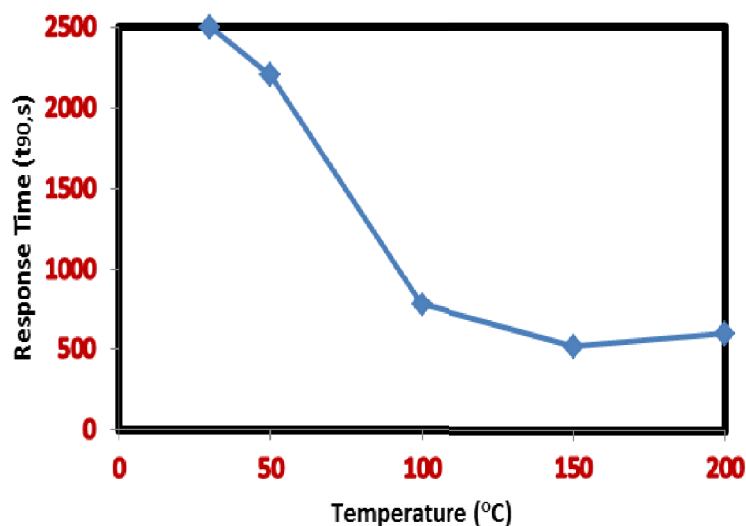
Figure 6.14. Response time versus temperature graph for 3 nm $Pt_{0.80}Ag_{0.20}$ thin film sensor exposed to 1000 ppm H_2 at 150 °C

Concentration dependent hydrogen sensing properties of PtAg sensors were also investigated at different temperature intervals. PtAg sensors exposed to different hydrogen concentrations from 25 ppm to 1000 ppm. After the PtAg films expose to every desired hydrogen gas concentration, the resistance of $Pt_{0.80}Ag_{0.20}$ thin film sensor decreased and came to saturation for all measurements. Then the measurement chamber was cleaned with dry air, the resistances of the PtAg sensor increased rapidly and the rate of increase reached saturation again. The best sensitivity measurement were performed at 150 °C for both $Pt_{0.80}Ag_{0.20}$ sensor because of reversibility performance and recovery time properties when exposed to hydrogen gas. Figure 6.15 shows the resistance versus time for 3 nm $Pt_{0.80}Ag_{0.20}$ sensor. It is clearly seen that the resistance of the PtAg sensor decreased with enhancing hydrogen concentration.
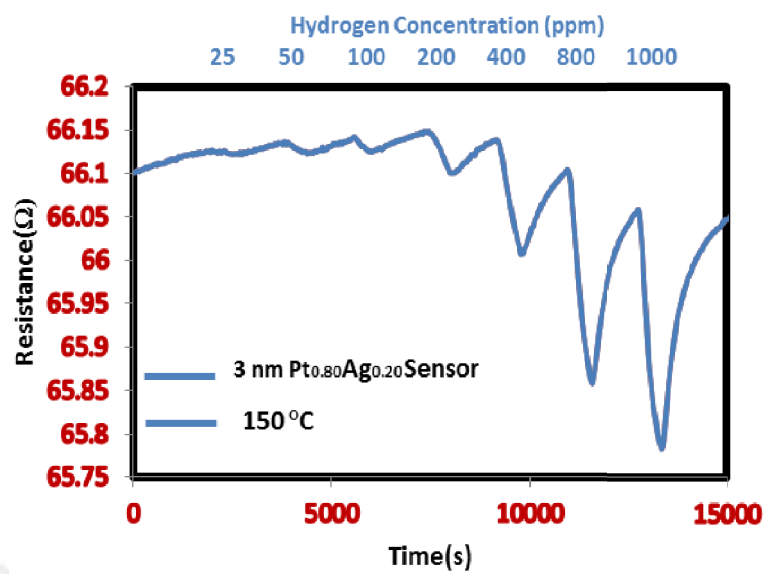
Figure 6.15. The resistance versus time graph for 3 nm Pt$_{0.80}$Ag$_{0.20}$ thin film sensor at 150 ºC

CHAPTER 7. CONCLUSIONS AND SUGGESTIONS FOR FUTURE WORKS

7.1. Conclusions

In this thesis, hydrogen gas sensing properties of Pt and PtAg thin film resistive sensors were investigated. The gas sensing mechanism of Pt based H_2 sensor was explained by the proposed mechanism.

Magnetron sputtering deposition technique was used to fabricate Pt and PtAg alloy thin films. The purpose of choosing sputtering technique is to make high quality Pt and PtAg thin film coating homogenously and rapidly. Pt thin films with different thicknesses such as 2 nm, 5 nm, 15 nm and 50 nm were prepared on a glass slide. On the other hand, 3 nm $Pt_{0.95}Ag_{0.05}$, $Pt_{0.90}Ag_{0.10}$ and $Pt_{0.80}Ag_{0.20}$ alloy thin films were fabricated and measured in the concentration range of 25 ppm and 1000 ppm H_2.

Fabricated Pt and PtAg thin films were characterized scanning electron microscopy (SEM), X-ray diffraction (XRD), X-ray photoelectron spectroscopy (XPS) and energy dispersive X-ray spectroscopy (EDX) techniques. SEM images shows that Pt films were coated homogeneously onto the glass slides by sputtering. There is no impurity on the Pt coated surfaces and it can be clearly seen in the XRD, EDX and XPS patterns. The results are well agreement with previous studies about platinum thin film grown via sputtering in literature.

Hydrogen sensing properties of the fabricated Pt and PtAg thin film sensors were investigated depending on thickness of thin film, hydrogen concentration and temperature. Pt and PtAg sensors, which have different film thicknesses and chemical composition ratios, were operated under different hydrogen concentrations and dry air flow. The H_2 gas sensing performances of Pt and PtAg sensors were

tested at a temperature range from 30 °C to 200 °C. The best working hydrogen sensor was detected in this way.

The temperature dependent resistance changes of the Pt and PtAg thin film sensors were also studied. The resistivities of Pt and PtAg sensors increased with increasing temperature. The resistances of the Pt sensors were inversely proportional to the thickness of Pt thin films. The results showed that 2 nm Pt thin film sensor exhibits the best hydrogen sensitivity at 30 °C. However the best response time was obtained after 100 °C for 2 nm Pt sensor. Among the PtAg thin film sensors, 3 nm $Pt_{0.80}Ag_{0.20}$ thin film sensor showed the best sensitivity and response time at 150 °C.

As a result, H_2 sensitivity of Pt thin film sensor has higher than that of PtAg sensor. Pt sensor works at room temperature while PtAg sensor needs for high temperature to work well. Improvements in working performance of PtAg sensor would depend on developing the fabrication process of PtAg thin films and some researches are necessary to enhance H_2 sensing sensitivities of PtAg sensor. On the other hand, the working performance of Pt sensor demonstrated that it can be used in desired application areas for hydrogen gas sensor technologies. The promising results presented in this study for hydrogen detection by using Pt as a sensing material.

7.2. Suggestions For Future Works

In this study, among the PtAg thin film sensors, the best sensing property was observed for $Pt_{0.80}Ag_{0.20}$ sensor. The results have shown that the chemical composition ratios of the the PtAg thin films affect the sensitivities of the films for hydrogen detection. PtAg thin films may have higher hydrogen sensitivity. In order to be sure about their H_2 sensing properties, different chemical ratios have to investigated by researcher. Beside, the thickness dependent studies of PtAg thin films will have to be done to detect better hydrogen sensitivity.

REFERENCES

[1]   Christofides, C. Mandelis, A. 1990. Solid-state sensors for trace hydrogen gas detection. Journal of Applied Physics, 68(6), R1-R30.

[2]   Korotcenkov, G. 2013. Handbook of gas sensor materials (pp. 49-116). Springer: New York, NY, USA.

[3]   Yamazoe, N. 2005. Toward innovations of gas sensor technology. Sensors and Actuators B: Chemical, 108(1), 2-14.

[4]   Hubert, T. Boon-Brett, l. Black, G. Banach, U. 2011. Hydrogen sensors– a review. Sensors and Actuators B: Chemical, 157(2), 329-352,

[5]   Guzelaydın, A. H. 2013. Investigation of gas sensing properties of nanoparticles functionalized with ferrocene molecules. Izmır Instıtue of Technology. Institue of Art and Science. Master Thesis.

[6]   Neri, G. 2015. First fifty years of chemoresistive gas sensors. Chemosensors, 3.1: 1-20.

[7]   Soundarrajan, P. Schweighardt, F. 2009. Hydrogen sensing and detection. In Hydrogen Fuel: Production, Transport, and Storage (pp. 495-534). CRC Press Boca Raton.

[8]   Bennaceur, K. Clark, B. Orr, Jr. F, M. Ramakrishnan, T. S, Roulet, C. Stout, E. 2005. Hydrogen: a future energy carrier? Gas, 25(20.1), 15-3.

[9]   Shukla, S. Seal, S. Ludwig, L. Parish, C. 2004. Nanocrystalline indium oxide-doped tin oxide thin film as low temperature hydrogen sensor. Sensors and Actuators B: Chemical, 97(2), 256-265.

[10]   Pitts, R. Liu, P. Lee, S. H, Tracy. E, Smith. R, D. Salter, C. 2001. Interfacial stability of thin film hydrogen sensors. In Proceedings of the DOE Hydrogen Program Review.

[11]   10 Reasons to Support Hydrogen and Fuel Cell Funding. 2011. http://www.chfca.ca/media/10_Reasons_Support_Funding.pdf,   Access Date: 20.02.2016.

[12]   http://www.chfca.ca/the-sector/sector-benefits/ Access Date: 13.05.2016.

[13]   Martínez-Orozco, R. D., Antaño-López, R. Rodríguez-González, V. 2015. Hydrogen-gas sensors based on graphene functionalized palladium nanoparticles: impedance response as a valuable sensor. New Journal of Chemistry, 39(10), 8044-8054.

[14]   htttp://www.vutbr.cz/www_base/zav_prace_soubor_verejne.php?file_id= 40087, Access Date: 06.01.2016.

[15]   Hord, J. Is hydrogen a safe fuel?.1978. International journal of hydrogen energy 3.2: 157-176.

[16]   Eichert, H. Fischer, M. 1986. Combustion-related safety aspects of hydrogen in energy applications. International journal of hydrogen energy, 11(2), 117-124.

[17]   Phase, I. 2008. Test Protocol Document, Hydrogen Safety Sensor Testing.

[18]   Kandasamy, S. 2007. Investigation of SiC based field effect sensors with gas sensitive metal oxide layers for hydrogen and hydrocarbon gas sensing at high temperatures. RMIT University, Melbourne, Australia. PhD Thesis.

[19]   Gu, H. Wang, Z. Hu, Y. 2012. Hydrogen gas sensors based on semiconductor oxide nanostructures. Sensors, 12(5), 5517-5550.

[20]   Schwandt, C. 2013. Solid state electrochemical hydrogen sensor for aluminium and aluminium alloy melts. Sensors and Actuators B: Chemical, 187, 227-233.

[21]   Electrochemical Sensors - International Sensor Technology http://www .intlsensor. com /pdf/electrochemical.pdf Access Date: 12.04.2016.

[22]   Brauns, E. Morsbach, E. Baumer, M. Lang, W. 2013. A fast and sensitive catalytic hydrogen sensor based on a stabilized nanoparticle catalyst. In Solid-State Sensors, Actuators and Microsystems (TRANSDUCERS & EUROSENSORS XXVII), 2013 Transducers & Eurosensors XXVII: The 17th International Conference on (pp. 1178-1181).

[23]   Petrová, L. 2011. Testing of hydrogen sensors based on organic materials, Brno University of Technology. Mater of Science Thesis.

[24]   Sluder. C, S. Storey. J, M. Lewis, S. A, Wagner. R, M. 2004. A thermal conductivity approach for measuring hydrogen in engine exhaust. SAE transactions, 113(4), 1614-1621.

[25]   Fisher, B, H. 2012. Surface acoustic wave (saw) cryogenic liquid and hydrogen gas sensors. University of Central Florida Orlando, Florida. Doctoral Dissertation.

[26]   El Gowini. M, M. Moussa. W, A. 2010. A finite element model of a MEMS-based surface acoustic wave hydrogen sensor. Sensors, 10(2), 1232-1250.

[27]   Pahwa. P, K. Pahwa. G, K. 2014. Hydrogen Economy. The Energy and Resources Institute (TERI).

[28]   Kiefer, T. Favier, F. Vazquez-Mena, O. Villanueva, G. Brugger, J. 2008. A single nanotrench in a palladium microwire for hydrogen detection. Nanotechnology, 19(12), 125502.

[29]   Ramanathan, M. Skudlarek, G. Wang, H. H, Darling. S, B. 2010. Crossover behavior in the hydrogen sensing mechanism for palladium ultrathin films. Nanotechnology, 21(12), 125501.

[30]   Offermans, P. Tong, H. D, Van Rijn. C, J. M, Merken. P, Brongersma. S, H. Crego-Calama, M. 2009. Ultralow-power hydrogen sensing with single palladium nanowires. Applied Physics Letters, 94(22), 223110.

[31]   Jeon, K. J. Lee. J, M. Lee, E. Lee, W. 2009. Individual Pd nanowire hydrogen sensors fabricated by electron-beam lithography. Nanotechnology,20(13), 135502.

[32]   Jeon, K. J, Jeun. M, Lee. E, Lee. J, M. Lee, K. I., von Allmen, P., & Lee, W. 2008. Finite size effect on hydrogen gas sensing performance in single Pd nanowires. Nanotechnology, 19(49), 495501.

[33]   Eisele, I. Doll, T. Burgmair, M. 2001. Low power gas detection with FET sensors. Sensors and Actuators B: Chemical, 78(1), 19-25.

[34]   Lu, C. 2009. Micro-Fabricated Hydrogen Sensors Operating at Elevated Temperatures. University of Kentucky. Doctoral Dissertation.

[35]   Tsukada, K. Kiwa, T. Yamaguchi, T. Migitaka, S. Goto, Y. Yokosawa, K. 2006. A study of fast response characteristics for hydrogen sensing with platinum FET sensor. Sensors and Actuators B: Chemical, 114(1), 158-163.

[36]   Scharnagl, K. Karthigeyan, A. Burgmair, M. Zimmer, M. Doll, T. Eisele, I. 2001. Low temperature hydrogen detection at high concentrations: comparison of platinum and iridium. Sensors and Actuators B: Chemical, 80(3), 163-168.

[37]   Yang, F. Donavan, K. C. Kung, S. C. Penner, R. M. 2012. The surface scattering-based detection of hydrogen in air using a platinum nanowire. Nano letters, 12(6), 2924-2930.

[38]   Abburi, A. Abrams, N. Yeh, W. J. 2012. Synthesis of nanoporous platinum thin films and application as hydrogen sensor. Journal of Porous Materials, 19(5), 543-549.

[39]   Patel, S. V. Gland, J. L. Schwank, J. W. 1999. Film structure and conductometric hydrogen-gas-sensing characteristics of ultrathin platinum films. Langmuir, 15(9), 3307-3311.

[40]   Machappa, T. Sasikala, M. Prasad, M. V. N. A. 2010. Design of Gas Sensor Setup and Study of Gas (LPG) Sensing Behavior of Conducting Polyaniline/Magnesium Chromate (MgCrO) Composites. Sensors Journal, IEEE, 10(4), 807-813.

[41]   West, A. R. 2007. Solid state chemistry and its applications. John Wiley & Sons.

[42]   Meric, Z. 2011. Antistatic applications: Metal coated fibers by magnetron sputtering. Izmır Instıtue of Technology. Instiue of Art and Science. Master Thesis.

[43]   Singh, A. V. Mehra, R. M. Buthrath, N. Wakahara, A. Yoshida, A. 2001. Highly conductive and transparent aluminum-doped zinc oxide thin films prepared by pulsed laser deposition in oxygen ambient. Journal of Applied Physics, 90(11), 5661-5665.

[44]   Hu, J. Gordon, R. G. 1992. Textured aluminum-doped zinc oxide thin films from atmospheric pressure chemical-vapor deposition. Journal of Applied Physics, 71(2), 880-890.

[45]   Tahar, R. B. H. Tahar, N. B. H. 2002. Mechanism of carrier transport in aluminum-doped zinc oxide. Journal of applied physics, 92(8), 4498-4501.

[46]   Kon, M. Song, P. K. Mitsui, A. Shigesato, Y. 2002. Crystallinity of gallium-doped zinc oxide films deposited by DC magnetron sputtering using Ar, Ne or Kr gas. Japanese journal of applied physics, 41(10R), 6174.

[47]   Depla, D. Mahieu, S. GREENE, J. 2010. Sputter deposition processes. Handbook of deposition technologies for films and coatings: science, applications and technology, 253-296.

[48]   Kelly, P. J. Arnell, R. D. 2000. Magnetron sputtering: a review of recent developments and applications. Vacuum, 56(3), 159-172.

[49]   http://www.ajaint.com/what-is-sputtering.html, Access Date: 23.02.2016.

[50]   http://www.directvacuum.com/pdf/what_is_sputtering.pdf, Access Date: 23.02.2016.

[51]   Carradò, A. Pelletier, H. ROLAND, T. 2011. Nanocrystalline thin ceramic films synthesised by pulsed laser deposition and magnetron sputtering on metal substrates for medical applications. INTECH Open Access Publisher.

[52]   https://en.wikipedia.org/wiki/Sputter_deposition, Access Date: 23.02. 2016.

[53]   https://www.leica-microsystems.com/science-lab/improvement-of metallic -thin-films-for-hr-sem-by- using-dc- magnetron-sputter-coater/ Access Date: 23.02.2016.

[54]   http://www.svc.org/DigitalLibrary/documents/2015.Fall.DJC.pdfAccess Date: 25.02.2016.

[55]   http://marriott.tistory.com/131, Access Date: 07.03.2016.

[56]   Walls, J. M. Smith, R. (EDS.). 2013. Surface science techniques. Elsevier.

[57]   Zhang, J. (ED.). 2008. PEM fuel cell electrocatalysts and catalyst layers: fundamentals and applications. Springer Science & Business Media.

[58]   http://surface-science.uni-graz.at/techniques/xps.htm, Access Date:10.04. 2016

[59]   http://ssrl.slac.stanford.edu/e-science.uni-gra/corelevel.html,Access Date: 10.04.2016.

[60]   http://www.cem.msu.edu/~cem924sg/Topic09.pdf, Access Date:10.04. 2016.

[61]   https://wiki.utep.edu/display/~agaribaldigarcia/Auger+Electron+ Spectroscopy, Access Date: 11.04.2016.

[62]   Mohai, M. 2005. Development and applications of quantitative X-ray photoelectron spectroscopy. University of Pannonia. Doctoral Dissertation.

[63]   http://2012books.lardbucket.org/books/principles-of-general-chemistry-v1.0/s16-solids.html, Access Date: 02.01.2016.

[64]   Moudgil, H. K. 2010. Textbook of Physical Chemistry. PHI Learning Pvt. Ltd.

[65]   https://commons.wikimedia.org/wiki/File:Bragg%27s_Law.PNG.Access Date: 25.04.2016.

[66]   http://www.kshitij-iitjee.com/diffraction-of-x-rays-by-crystals.Access Date: 25.04.2016.

[67]   Clemeña, G. G. Virmani, Y. P. Stoner, G. E. Kelly, R. G. 2002. Electrochemical chloride extraction: influence of concrete surface on treatment (No. FHWA-RD-02-107,). US Department of Transportation, Federal Highway Administration, Research, Development, and Technology, Turner-Fairbank Highway Research Center.

[68]   https://www.researchgate.net/file.PostFileLoader.html?id=52d989f9cf57d7f82a8b4630&assetKey=AS%3A272425437073409%401441 962693 691. Access Date: 02.05.2016.

[69]   Kallehauge, Jesper F. 2007.Measurements of surface conductivity using micro four point probes. Institut for Fysik og Astronomi, Aarhus Universitet. Master of Science Thesis.

[70]   Santos, J. P. Fernández, M. J. Fontecha, J. L. Matatagui, D. Sayago, I. Horrillo, M. C. Gracia, I. 2014. Nanocrystalline Tin Oxide Nanofibers Deposited by a Novel Focused Electrospinning Method. Application to the Detection of TATP Precursors. Sensors, 14(12), 24231-24243.

[71]   Dao, A. T. N. Mott, D. M. Higashimine, K. Maenosono, S. 2013. Enhanced electronic properties of Pt@ Ag heterostructured nanoparticles. Sensors, 13(6), 7813-7826.

[72]   Chang, I. Woo, S. Lee, M. H. Shim, J. H. Piao, Y. Cha, S. W. 2013. Characterization of porous Pt films deposited via sputtering. Applied Surface Science, 282, 463-466.

[73]   Geyer, S. M. Methaapanon, R. Johnson, R. Brennan, S. Toney, M. F. Clemens, B. Bent, S. 2014. Structural evolution of platinum thin films grown by atomic layer deposition. Journal of Applied Physics, 116(6), 064905.

[74]   Aaltonen, T. Ritala, M. Sajavaara, T. Keinonen, J. Leskelä, M. 2003. Atomic layer deposition of platinum thin films. Chemistry of materials, 15(9), 1924-1928.

[75]   Hecq, A. Delrue, J. P. Hecq, M. Robert, T. 1981. Sputtering deposition, XPS and X-ray diffraction characterization of hard nitrogen-platinum thin films. Journal of Materials Science, 16(2), 407-412.

[76]   J.F. Moulder, J. Chastain. 1992. Handbook of X-ray Photoelectron Spectroscopy: A Reference Book of Standard Spectra for Identification and Interpretation of XPS Data, Physical Electronics Division, Perkin-Elmer Corporation.

[77]   K, Benaissi. L, Johnson. D. A, Walsh. W, Thielemans. 2010. Synthesis of platinum nanoparticles using cellulosic reducing agents. Green Chem 12, 220-222.

[78]   Y.M. Sun, D.N. Belton, J.M. White. 1986. Characteristics of platinum thin films on titanium dioxide (110). The Journal of Physical Chemistry 90, 5178-5182.

[79]   H.-W. Yoo, S.Y. Cho, H.J. Jeon, H.T. Jung. 2015. Well-Defined and High Resolution Pt Nanowire Arrays for a High Performance Hydrogen Sensor by a Surface Scattering Phenomenon. Analytical Chemistry 87, 1480-1484.

[80]   C, Sachs. M, Hildebrand. S, Völkening. J, Wintterlin. G, Ertl. 2001. Spatiotemporal Self-Organization in a Surface Reaction: From the Atomic to the Mesoscopic Scale. Science 293, 1635-1638.

[81]   K.M. Ogle. J.M. White. 1984. The low temperature water formation reaction on Pt (111): A static SIMS and TDS study. Surface Science 139, 43-62.

[82]   J.L, Gland. G.B, Fisher. E.B, Kollin. 1982. The hydrogen-oxygen reaction over the Pt(111) surface: Transient titration of adsorbed oxygen with hydrogen. Journal of Catalysis 77, 263-278.

RESUME

Şeyma Ürdem was born in August 16, 1991, in Sakarya. She completed her primary and high school education in Sakarya. She graduated from Chemistry Department of Abant Izzet Baysal University in 2014. She attended master science program in Nanoscience and Nanoengineering at Sakarya University in 2014. She was assigned as a project assistant in a TUBITAK project which is called, 'Fabrication and Characterization of Nanostructured Pt and Pt Alloys, and Investigation of Their Hydrogen Gas Sensing Properties'. She currently works as a project assistant.